TECHNICAL UNIVERSITY OF LIBEREC
Faculty of Textile Engineering

Influence of High Temperatures on Properties of Geopolymers Filled by Inorganic Fibrous Particles

Dissertation Thesis

Study programme:	P3106 Textile Engineering
Study branch:	Textile Technics and Materials Engineering
Author:	**Promoda Kumar Behera**
Thesis Supervisor:	prof. Ing. Jiří Militký, CSc. Department of material engineering

Liberec 2019

Declaration

I hereby certify I have been informed that my dissertation is fully governed by Act No. 121/2000 Coll., the Copyright Act, in particular Article 60 – School Work.

I acknowledge that the Technical University of Liberec does not infringe my copyrights by using my dissertation for internal purposes of the Technical University of Liberec.

I am aware of my obligation to inform the Technical University of Liberec on having used or granted license to use the results of my dissertation; in such a case the Technical University of Liberec may require reimbursement of the costs incurred for creating the result up to their actual amount.

I, myself, have written my dissertation as an original and primary work using the literature listed below and consulting it with my thesis supervisor and my thesis counsellor.

At the same time, I honestly declare that the texts of the printed version of my dissertation and of the electronic version uploaded into the IS/STAG are identical.

July 29, 2019 Promoda Kumar Behera

ABSTRACT

The presented research work deals with elevated temperature properties of inorganic fibrous particles filled geopolymers when exposed to 200, 400 and 800 ^{o}C. The basalt fibrous wastes and carbon fibrous particles (Carbiso) were chosen as source of inorganic fibrous particles due to their less cost and better thermal resistance properties. The high energy ball milling process was employed to prepare basalt microfibrils (BMF) and carbon microfibers (CMF) after 30 min dry pulverization of basalt fibrous wastes and carbiso powder, respectively. The prolonged pulverization was not continued because of rise in temperature of ball mill and sticking of particles to the surface of milling containers. Nevertheless, the longer grinding of carbiso powder showed less sticking tendency as compared to basalt fibrous wastes. Later, the milled particles were incorporated under 5, 10 and 15 wt % loading into geopolymers synthesized from calcined kaolin and shale clay residues. The prepared BMF/geopolymer composites or CMF/geopolymer composites were then evaluated for physical properties, micro-structural analysis and compression strength before and after exposure to elevated temperatures. As compared to BMF, the addition of CMF was found to maintain compact structure of geopolymers at elevated temperature exposures. This behavior was attributed to effective pore filling ability and better thermo-chemical resistance of CMF as compared to BMF. The geopolymer composite of 10 wt % BMF depicted the maximum compressive strengths of 34 MPa, 42 MPa, 23 MPa and 16 MPa at 30 ^{o}C, 200 ^{o}C, 400 ^{o}C and 800 ^{o}C, respectively. On the other hand, the maximum compressive strengths of 44 MPa, 49 MPa, 30 MPa and 21 MPa was recorded for the geopolymer composite of 10 wt % CMF at 30 ^{o}C, 200 ^{o}C, 400 ^{o}C and 800 ^{o}C, respectively. This indicated greater decrease in thermal stresses as well as more restriction on swelling of unreacted precursor phases after addition of CMF than BMF. Furthermore, the geopolymers filled by BMF and CMF

showed higher compression strength values than the previously reported results on neat OPC when exposed to 800 ^{o}C. The 5, 10 and 15 wt% BMF filled geopolymers showed 22 %, 42 %, and 34 % increase over OPC respectively, whereas 5, 10 and 15 wt% CMF filled geopolymers showed 76 %, 88 % and 112 % increase over OPC respectively.

Keywords: Filled geopolymers, Basalt microfibrils, Carbon microfibers, Geopolymer composites, Compressive strength, Pore-filling ability, Thermal resistance

ABSTRAKT

Předložená práce se zabývá chováním geopolymerů plněných anorganickými vlákennými částicemi při zvýšené teplotě 200, 400 a 800 ^{o}C. Čedičový vláknitý odpad Pro výběr anorganických plniv byl zohledněn požadavek zvýšené tepelné odolnosti při přijatelné ceně a možnosti mechanického zjemňování. Byly vybrány částice na bázi čedičového vláknitého odpadu auhlíkové vlákenné částice (Carbiso). Pro přípravu čedičových mikrofibril (BMF) a uhlíkových mikrovláken (CMF) bylo použito vysoce energetické mletí za sucha v kulovém mlýnku. Doba mletí 30 min. byla specifikována s ohledem na omezení vzrůstu teploty mlýnku a zabránění lepivosti mletých částic na jeho vnitřní povrch. Byly syntetizovány geopolymery z kalcinovaného kaolinu a břidlicového jílu s obsahem mletých částic BMF a CMF v rozmezí 5, 10 a 15% hmotnostních procent. Takto připravené kompozitní materiály geopolymer/CMF a geopolymer/BMF byly charakterizovány pomocí fyzikálních vlastností, mikrostrukturní analýzy a pevnosti v tlaku před a po vystavení zvýšeným teplotám. Bylo zjištěno, že přidání CMF udržuje lépe kompaktní strukturu kompozitních materiálů při zvýšených teplotních expozicích než přidání BMF. Tento rozdíl v chování obou plniv souvisí s jejich schopností efektivně plnit póry a termo chemickou degradací BFM za vysokých teplot. Kompozit s obsahem 10 hmotnostních procent BMF docílil pevnost tlaku 34 MPa, 42 MPa, 23 MPa and 16 MPa při teplotách 30 ^{o}C, 200 ^{o}C, 400 ^{o}C and 800 ^{o}C, Kompozit s obsahem 10 hmotnostních procent CMF docílil pevnost v tlaku 44 MPa, 49 MPa, 30 MPa a 21 MPa při teplotách 30 ^{o}C, 200 ^{o}C, 400 ^{o}C a 800 ^{o}C. Je patrné, že přídavek anorganických vláknitých částic přispívá ke snížení tepelného napětí a omezuje bobtnání nezreagované fáze prekurzoru. Geopolymrey plněné oběma typy částic vykazovaly zvýšené hodnoty pevnosti v tlaku v porovnání s geopolymery bez obsahu částicových plniv při teplotě 800 ^{o}C. Geopolymery s obsahem 5, 10 a 15 hmotnostních procent

BMF vykazovaly 22 %, 42 %, a 34 % nárůst pevnosti v tlaku ve srovnání s geopolymery bez obsahu částicových plniv. Geopolymery s obsahem 5, 10 a 15 hmotnostních procent CMF vykazovaly 76 %, 88 % and 112 % nárůst pevnosti v tlaku ve srovnání s geopolymery bez obsahu částicových plniv.

Klíčová slova: Plněné geopolymery, čedičová mikrovlákna, Uhlíková mikrovlákna, Geopolymerní kompozity, Pevnost v tlaku, Schopnost plnění pórů, Tepelná odolnost

ACKNOWLEDGEMENT

This research was carried out in the Department of Material Engineering (KMI) at Faculty of Textile Engineering in Technical University of Liberec, Czech Republic. I would like to thank everyone who has motivated, influenced and contributed to my life in many remarkable ways. First and foremost, I would like to express my sincere respect and appreciation to my supervisor Prof. Ing. Jiri Militky, CSc. EURING, for his inspiration, guidance and giving me an opportunity to work under his kind supervision. I want to say special thanks to Dr Vijay Baheti, PhD for his time-to-time suggestions and help during my entire research work. He has been encouraging and supportive throughout my entire time at Technical University of Liberec. In the absence of financial support, this research would not have been possible; I, therefore, thank Ing. Jana Drasarova, Ph.D (Dean of the Faculty of Textile Engineering); Ing. Gabriela Krupincova, PhD (Vice-Dean for Science and Research), Ing. Pavla Tesinova, PhD (Vice-Dean for international affairs) and Dr. Blanka Tomkova (HOD, Department of Materials Engineering) for their kind support, conference attendance and mobility funds where necessary such that this work may be done and progresses to another level. I am also grateful to Prof. Holmer Savastano Junior for guiding me during my internship stay at Department of Biosystems Engineering (ZEB), University of Sao Paulo, Pirassununga, Brazil. I would also like to thank Ing. Hana Musilová, Bohumila Keilová, Martina Čimburová and Jana Grabmüllerová for their regular help and support. Last but not least, a special thanks to my parents for their unwavering support in spirit and livelihood.

Promoda Kumar Behera

LIST OF ACRONYMS

OPC	Ordinary Portland Cement
G	Geopolymer
BMF	Basalt micro fibril
CMF	Carbon micro fibril
SEM	Scanning electron microscope
EDS	Energy-dispersive X-ray spectroscopy
XRD	X-Ray Diffraction
TGA	Thermal gravimetric analysis
CSH	Calcium-Silicate-Hydrate
CASH	Calcium-Alumino-Silicate-Hydrate
NASH	Sodium-Alumino-Silicate-Hydrate
QP	Quartz powder
HV	Vickers hardness

LIST OF TABLES

LIST OF FIGURES

TABLE OF CONTENTS

1 CHAPTER: INTRODUCTION

There has been an increased environmental concern related to manufacture of ordinary Portland cement (OPC) as it results in significant release of CO_2, rapid depletion of landscape, dust production during transport, and generation of noise, etc [1–4]. Moreover, OPC has shown inferior performance in sulphate or acid environment due to easy dissolution of calcium compounds [5]. As a result, the research over alternative OPC binders gained importance to achieve environmental sustainability and durability in construction and building industry [1,6]. For the first time in 1939, Feret carried out the activation of ground blast furnace slags with sodium hydroxide solutions to produce cementitious materials suitable for concrete production [7]. Later on, number of studies was performed to develop alkali-activated cements (see Table 1), which were mentioned in literature with different terminologies such as 'geopolymers', 'mineral polymers', 'geocements', 'inorganic polymers', 'inorganic polymer glasses', 'alkali-bonded ceramics', 'alkali ash material', 'soil cements', 'hydroceramics', etc [8]. In 1970, Joseph Davidovits coined the term 'geopolymer' to a class of solid materials synthesized by the reaction of an aluminosilicate powder with an alkaline solution [9]. Geopolymer is considered as the third generation cement after lime and OPC, and it is now emerged as an alternative to OPC due to superior durability and environmental performance [10]. Figure 1 shows geopolymers to be part of the alkali activated family of cementitious materials, characterized by low calcium content.

Table 1. History of developments of alkali-activated cements [10].

Author	Year	Significance
Feret	1939	Slags used for cement
Purdon	1940	Alkali–slag combinations
Glukhovsky	1959	Theoretical basis and development of alkaline cements
Glukhovsky	1965	First called “alkaline cements”
Davidovits	1979	“Geopolymer” term
Malinowski	1979	Ancient aqueducts characterized
Forss	1983	F-cement (slag–alkali–superplasticizer)
Langton and Roy	1984	Ancient building materials characterized
Davidovits	1985	Patent of “Pyrament” cement
Krivenko	1986	DSc thesis, R_2O–RO–SiO_2–H_2O
Malolepsy and Petri	1986	Activation of synthetic melilite slags
Malek et al.	1986	Slag cement-low level radioactive wastes forms
Davidovits	1987	Ancient and modern concretes compared
Deja and Malolepsy	1989	Resistance to chlorides shown
Kaushal et al.	1989	Adiabatic cured nuclear wastes forms from alkaline mixtures
Roy and Langton	1989	Ancient concretes analogs
Majundar et al.	1989	$C_{12}A_7$–slag activation
Talling	1989	Alkali-activated slag
Wu et al.	1990	Activation of slag cement
Roy et al.	1991	Rapid setting alkali-activated cements
Roy and Silsbee	1992	Alkali-activated cements: an overview

Palomo and Glasser	1992	CBC with metakaolin
Roy and Malek	1993	Slag cement
Glukhovsky	1994	Ancient, modern and future concretes
Krivenko	1994	Alkaline cements
Wang and Scivener	1995	Slag and alkali-activated microstructure
Shi	1996	Strength, pore structure, permeability of alkali-activated slag
Fernández-Jiménez	1997	Kinetic studies of alkali-activated slag cements
Katz	1998	Microstructure of alkali-activated fly ash
Davidovits	1999	Chemistry of geopolymeric systems, technology
Roy	1999	Opportunities and challenges of alkali-activated cements
Palomo	1999	Alkali-activated fly ash — a cement for the future
Gong and Yang	2000	Alkali-activated red mud–slag cement
Puertas	2000	Alkali-activated fly ash/slag cement
Bakharev	2001	Alkali-activated slag concrete
Palomo and Palacios	2003	Immobilization of hazardous wastes
Grutzeck	2004	Zeolite formation
Sun	2006	Sialite technology
Duxson	2007	Geopolymer technology: the current state of the art
Hajimohammadi	2008	One-part geopolymer
Provis and Deventer	2009	Geopolymers: structure, properties and industrial applications

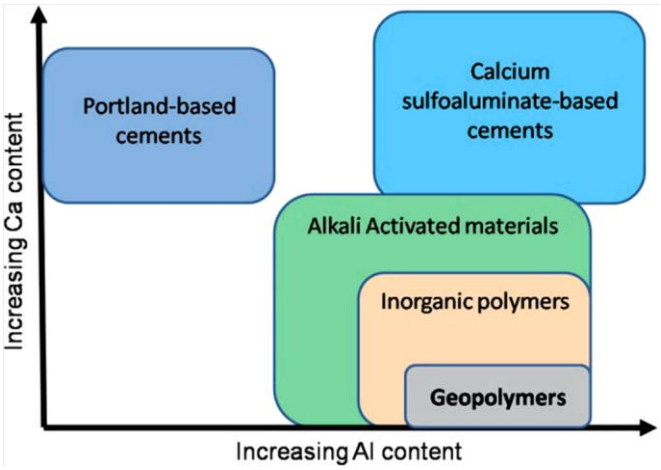

Figure 1. Relationship of geopolymers with Portland and other cements [7,11].

Compared to the traditional OPC, the geopolymers have following advantages [1,12–14].

a) ***Excellent mechanical property.*** It results from the presence of three-dimensional network structure and framework of $[\mathrm{Si-O-Al-O}]_n$ in geopolymers [15].

b) ***High durability.*** It results from the presence of inorganic materials containing massive zeolite-like minerals, such as sodalite $[\mathrm{Na}_n(\mathrm{Si-O-Al-O-})_n]$, analcime $[(\mathrm{Na,\ Ca,\ Mg})_n(\mathrm{Si-O-Al-O-})_n]$, etc [13].

c) ***Good chemical, fire and thermal resistance.*** It results from the acid resistance of $\mathrm{Si-O}$ and $\mathrm{Al-O}$ bonds, high temperature stability of oxide network structure and low thermal conductivity (0.24–0.38 W/(m·K)) values [14].

d) ***Fast curing speed and high interfacial binding force.*** It results from the rapid gel formation and early dehydration process [1,16].

e) ***Low cost and extensive sources.*** Relevant minerals are readily available, inexpensive and can be obtained from industrial wastes. Their contents in the earth's crust are 26.3% silicon, 7.73% aluminum and 48.6% oxygen [17,18].

f) ***Potential application of special structure.*** The silicon tetrahedral $(Si(OH)_4^-)$ and aluminum tetrahedral $(Al(OH)_4^-)$ form ring chain structures, which eventually results in multifunctional application (i.e. building materials processing, nuclear waste disposal, heavy metal immobilization and novel inorganic membrane manufacture) [19,20].

g) ***Low resource consumption and low CO_2 emission.*** Compared to traditional cement manufacture, the production of geopolymer saves 80% energy and reduces around 50–80 % CO_2 emissions [15,21].

h) ***Wide variety of potential applications.*** Thermal shock refractories, Fire resistant materials, thermal insulation, low energy ceramic tiles, high-tech composites for aircraft interior and automobile, refractory items, decorative stone artifacts, bio-technologies (materials for medical applications), high-tech resin systems, composites for infrastructures repair and strengthening, cements and concretes, low-tech building materials, cultural heritage, radioactive and toxic waste containment, archaeology and history of sciences, arts and decoration, foundry industry [19].

2 CHAPTER: THESIS SIGNIFICANCE, SCOPE AND OBJECTIVES

Geopolymers-based materials are very attractive in construction industry as green concrete due to their corrosion resistance, cost efficiency, low permeability, low density, low shrinkage, rapid strength gain rate, chemical stability and freeze-thaw resistance, etc [22]. However, they have certain limitations over OPC. Geopolymers tend to be brittle, vulnerable to crack formation and undergo catastrophic failure because of their cross-linked structure [23]. The inclusion of different fibers have shown to be effective in controlling crack propagation and enhancing the fracture energy of geopolymers, but the mechanical properties of geopolymers were found inadequate and non-consistent while exposed to elevated temperatures [24,25]. During fire accidents, various fibers fail in providing effective reinforcements owing to lack of durability and structural strength at higher temperature. Furthermore, the thermal expansion mismatch between fiber and matrix can introduce thermal fatigue and stresses, and therefore affect the lifetime and dimensional stability of the composites [8,26]. Moreover, the destruction of geopolymers can occur during the fire exposure due to evaporation of water adsorbed by N-A-S-H gel, formation of anhydrous products, crystallization of stable anhydrous phases and melting [27] (see Figure 2). Hence, more research is necessary to identify alternative fibers which have better thermal resistance and sustain higher residual mechanical properties while exposed to elevated temperature [28].

$$\underset{\text{Geopolymer}}{M_n[-(SiO_2)_z - AlO]_n . wH_2O} \xrightarrow{\text{Dehydration } 125-160\,^{\circ}C} \underset{\text{Anhydrous product}}{M_n[-(SiO_2)_z - AlO]_n}$$

$$\underset{\text{Anhydrous product}}{M_n[-(SiO_2)_z - AlO]_n} \xrightarrow{\text{Crystallization } 600-800\,^{\circ}C} \underset{\text{(Nepheline)}}{Na_2O.Al_2O_2.2SiO_2} \xrightarrow[\text{Recrystallization}]{\text{Above } 800\,^{\circ}C} \underset{\text{(Albite)}}{Na_2O.Al_2O_3.2SiO_2}$$

Figure 2. Geopolymer phase transformation during fire [27].

Many researchers studied the mechanical properties of glass fiber reinforced geopolymer mortar at high temperatures, whereas only few studies were reported on the basalt fibers [29,30]. The basalt fibers are easy to process, non-toxic, natural, eco-friendly and inexpensive as compared to other inorganic fibers. They are prepared from volcanic rocks produced from frozen lava, with a melting temperature comprised between 1500 and 1700 ^{o}C. They have extremely good modulus, high strength, improved strain to failure, high temperature resistance, excellent stability, good chemical resistance and reduced thermal and electrical conductivity [31,32]. Various researches reported on continuous basalt fabric or basalt fiber as a strengthening material for cementitious concrete structures, though there are confined studies on the consequence of short basalt fibers on the properties of geopolymers. In recent times, carbon materials are treated as a potential candidate for reinforcement of geopolymers while exposed to higher temperature because of their remarkable thermal, mechanical and electrical properties [33,34]. For this purpose, graphene, carbon nanofibers, carbon nanotubes etc were examined for enhancing the strength and ductility of geopolymer composites [35]. Furthermore, only some researchers also suggested the use of economical micro-size carbonized coconut shell, hemp hurds and bamboo particles particles over carbon nanotubes owing to their easier handling [36]. However, no research work is reported on the elevated temperature properties of carbiso particles filled geopolymers. The carbiso are 100 μm milled inexpensive carbon particles obtained from recycled carbon fibrous wastes.

The thesis systematically investigated the effects of incorporation of inexpensive inorganic microfibers (basalt microfibrils and carbon microfibers) on the structure and thermal evolution of geopolymers synthesized from metakaoline. The high energy ball milling process was employed to pulverize basalt fibrous wastes and carbiso into BMF and CMF, respectively.

Thereafter, the geopolymer composites were prepared by addition of 5, 10 and 15 wt% of BMF or CMF into metakaoline based geopolymers. The effect of BMF and CMF was separately studied on the change in microstructure, mechanical properties and toughening mechanisms of geopolymers after exposure to the elevated temperatures of 200°C, 400°C and 800°C. In particular, the following objectives were studied in detail

a) Effect of ball milling time on particle size distribution of BMF and CMF
b) Characterization of microstructure of geopolymer composites by SEM, EDS, Image analysis, XRD, TGA
c) Characterization of mechanical properties of geopolymer composites by measurement of compression strength, hardness, density, etc.
d) Evaluation of elevated temperature properties of geopolymer composites
e) Study of pore-filling ability of basalt microfibrils and carbon microfibers in geopolymer composites when exposed to elevated temperatures
f) Comparison of elevated temperature performance of geopolymer composites over previously reported traditional OPC based construction materials

3 CHAPTER: LITERATURE REVIEW

3.1 Geopolymer

Geopolymers are aluminosilicate materials with three-dimensional amorphous microstructure [6,37]. The natural minerals (i.e. metakaoline, laterite, and illite smectite clays) or industrial and agricultural waste materials (i.e. fly ash, sludge and rice husk ash) have been used as source of aluminosilicate for geopolymer preparation [8]. The fabrication of geopolymer using alkaline solution and aluminosilicate materials can be seen from Figure 3.

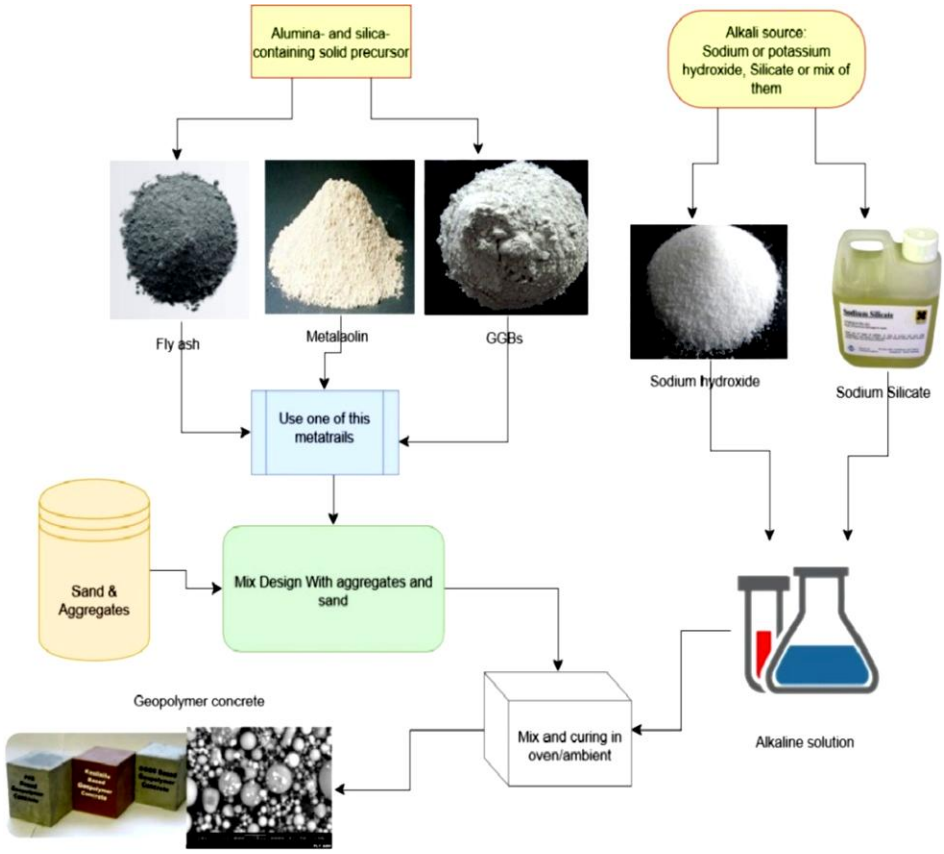

Figure 3. Steps in geopolymer production [6].

Figure 4 shows the structural model of the geopolymer, where the Al, H, Na, O and Si atoms are showed in silver, beige, yellow, red and blue, respectively. The polymerization of

silicon and aluminum tetrahedra precursors with the alkali or alkaline earth metal cations was reported to provide the charge balancing to the Al(IV) co-ordinated anion [38]. The oxides of aluminium and silicon minerals or aluminosilicates reacted with alkaline solution to make polymeric Si–O–Al bonds throughout the geopolymerization [39]. Later, the 'sialate' nomenclature was introduced by Davidovits to describe aluminosilicate structures according to their Si/Al ratio, with a ratio of 1.0 being a poly(sialate), 2.0 being a poly(sialate-siloxo), and 3.0 a poly(sialate-disiloxo) (see Figure 5) [40]. The linkage type Si-O-Si was named a siloxo bond, and Si-O-Al a sialate bond. The empirical formula of Poly(sialates) is as follow: $Mn\text{-}SiO_{2z}\text{-}AlO_{2n},wH_2O$, where z is the Si/Al molar ratio, M is an alkali cation, n is the polymerization degree, and w is the water content [41].

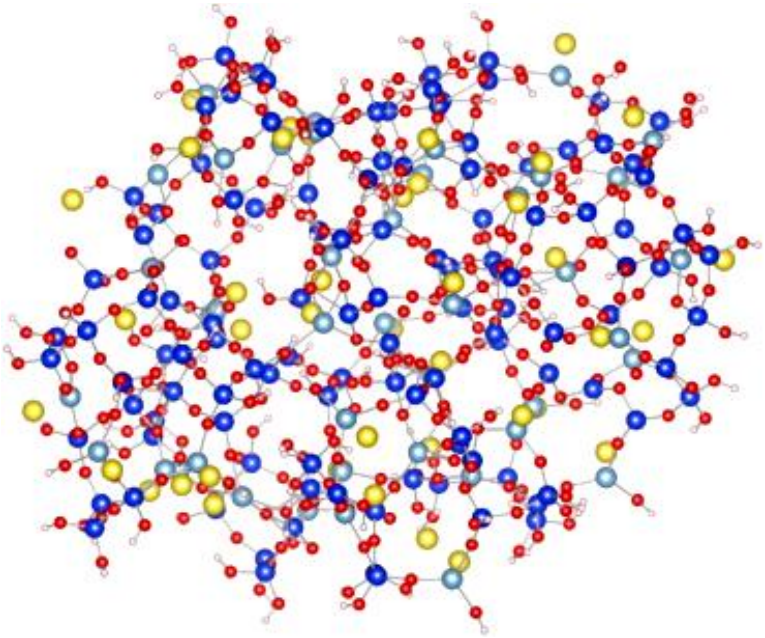

Figure 4. Structural model for geopolymers [38].

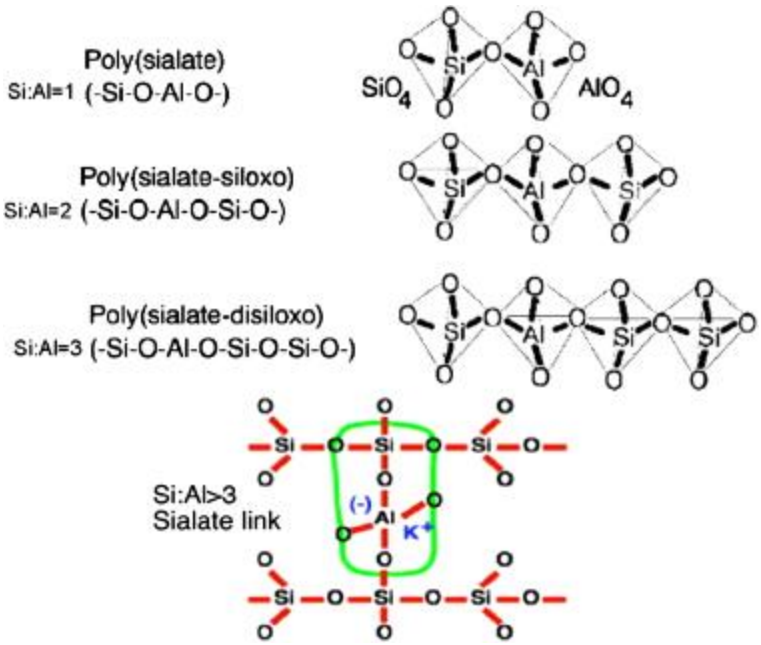

Figure 5. Poly(sialates) structures [41,42].

3.2 Mechanism of geopolymerization

The geopolymer preparation constitutes the reaction series between alkali sources and the solid precursors, and includes dissolution, precipitation, reorganization, gelation and polycondensation steps [38]. The simplified reaction mechanism for geopolymer preparation according to Duxson et al. can be seen from Figure 6(a). When the precursor and the alkali activator come in contact, the amorphous components (silicates and aluminates) of the precursor dissolve and inter-react to form an aluminosilicate gel. At first, aluminum-rich gel (Gel 1) is formed due to rapid dissolution of the reactive aluminum than the silicon. However, when more silicon dissolves in the later stage, the gel structure is reorganized to form the zeolite precursor gel (Gel 2). The gel 2 is more stable than the gel 1 due to formation of Si-O bonds than Al-O bonds. The reorganization processes continue and result in formation of some crystallized zeolite (i.e. solid mass similar to the hydration of OPC) [6]. Similary, Glukhovsky described the mechanism of alkali-activation as conjoined reactions of destruction–condensation, that include

the destruction of the prime material into low stable structural units, their interaction with coagulation structures and the creation of condensation structures (see Figure 6(b)) [10].

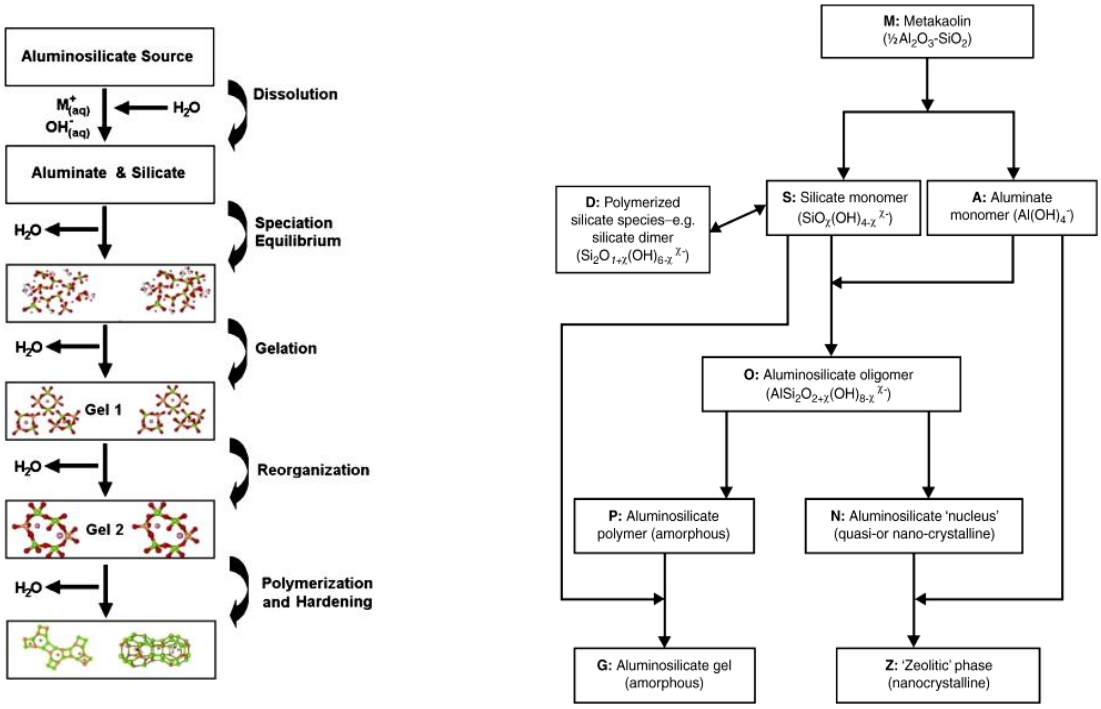

(a) Conceptual model [10,38] (b) Reaction processes [10]

Figure 6. Mechanism of geopolymerization

Davidovits suggested geopolymer preparation as an exothermic process, where the synthesis was performed through oligomers (dimer, trimer) to give the actual unit structures of the three-dimensional macromolecular edifices (see Figure 7). The synthesis of geopolymers is governed by a polycondensation reaction between silica and alumina precursors, where a partial substitution of Si^{4+} with Al^{3+} takes place, subsequently a complete ionic-balance with the Na^{+}/K^{+} of the NaOH/KOH (alkaline activator) [43]. The formation of enlarged Al-O-Si network results in high bond strength of ~3.02 kJ/mol due to some extent covalent bonds linked with the Si-O, Al-O and highly ionic Na-O pairs present in geopolymers [43]. The consequent network can give considerable structural strength (i.e. 30 MPa) at room temperature after ~24 h of synthesis of

geopolymers. Moreover, the presence of Calcium (~3 wt%) in geopolymers enables its ambient temperature curing, and therefore allows cleaner production compared to other ceramics [44]. Table 2 illustrates the chemical reactions during the typical steps of aluminosilicate framework transformation to geopolymer solid structure [44].

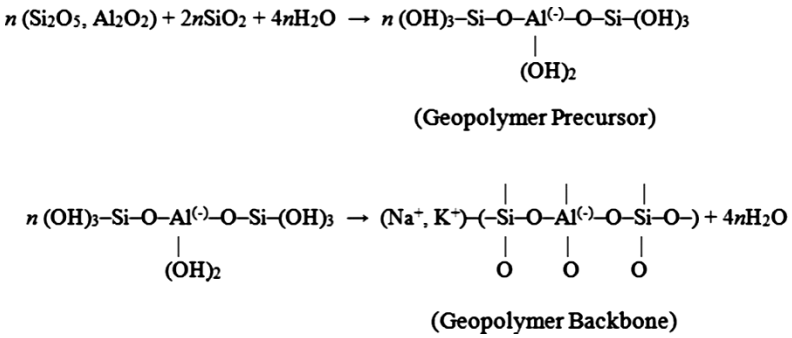

Figure 7. Aluminosilicate framework transformation to geopolymer solid structure [45,46].

Table 2. Chemical reactions of transformation of aluminosilicate materials to geopolymers [44].

Reaction stage	**Geopolymer phase**	**Reaction mechanism**
Aluminosilicate dissolution and separation into alumina and silicate ends	poly(sialate)	$n(Si_2O_5, Al_2O_2) + nH_2O + NaOH/KOH \rightarrow n(OH)_3\text{-}Si\text{-}O\text{-}Al(OH)_3 + Na^+/K^+$
	Poly(sialate-siloxo)	$n(Si_2O_5, Al_2O_2) + nSiO_2 + nH_2O + NaOH/KOH \rightarrow n(OH)_3\text{-}Si\text{-}O\text{-}Al^-\text{-}O\text{-}Si\text{-}(OH)_3 + Na^+/K^+$
Polycondensation/polymerization	Poly(sialate)	$n(OH)_3\text{-}Si\text{-}O\text{-}Al(OH)_3 + NaOH/KOH \rightarrow (Na^+/K^+)\text{-}(Si^{-}\text{-}O\text{-}Al^-\text{-}O\text{-})n + nH_2O$
	Poly(sialate-siloxo)	$n(OH)_3\text{-}Si\text{-}O\text{-}Al^-\text{-}O\text{-}Si\text{-}(OH)_3 + NaOH/KOH \rightarrow (Na^+/K^+)\text{-}(Si^{-}\text{-}O\text{-}Al^-\text{-}O\text{-}Si^-\text{-}O\text{-})_n + nH_2O$

3.3 Geopolymer performance

The strength of geopolymers rely on amorphous nature of geopolymers, distribution of undissolved Al–Si particle sizes, ratio of gel phase/undissolved Al–Si particles, gel phase strength and surface reaction between undissolved Al–Si particles and gel phase [47,48]. The development of compression strength depends on the molar Si/Al ratio during alkaline dissolution of the individual minerals [49]. Wang have reported increase in the compressive strength with the increase of sodium hydroxide concentration [50], which was ascribed to the improved dissolution of the metakaolinite particulates and thus the accelerated condensation of the monomer in the presence of higher sodium hydroxide concentration. Previous studies recorded the higher strength values when the ratios SiO_2/Al_2O_3 and Na_2O/Al_2O_3 were 3.0–3.8 and about 1, respectively [51]. In general, the properties and the structure of geopolymers can be elucidated by difference in the source Si/Al amorphous molar ratio, alkali metal cation type and concentration, water content and curing regime used in the geopolymer synthesis [7].

Role of precursors. For development of stable geopolymer, the source materials should be extremely amorphous and have low water demand, sufficient reactive glassy content and be capable of release aluminum easily [8]. The geopolymers prepared from different aluminosilicate sources show different chemical properties and microstructures due to change in chemical make-up, fineness, morphology, glassy phase content and mineralogical composition [8]. The metakaoline based geopolymer provides permeability, better strength, etc. But, it has drawbacks of poor rheological properties by reason of complex processing, plate shaped morphology, accelerated hydration reactions, higher water demand and more heat evolved at early ages [52]. Conversely, metakaoline-based geopolymer is less stronger and durable than that of fly ash-

based geopolymer. But, fly ash-based geopolymer has also disadvantages such as slow strength development, low early-age strength, extended setting times, construction delay, complexities to use in cold weather concreting, etc [27]. The benefits of slag-based geopolymer are better acid resistance and great early strength than those of fly-ash and metakaoline-based systems. Though, the slag being by-product of the ore refinement process, it is not easily obtainable. Moreover, the harder nature of slag requires frequent maintenance of equipments and costly processing than metakaoline and fly ash [53,54].

Role of alkali metals. Alkaline solutions are used for activation of the source materials during geopolymerization process. The combination of potassium silicate (K_2SiO_3) or sodium silicate (Na_2SiO_3) and potassium hydroxide (KOH) or sodium hydroxide (NaOH) is commonly employed as alkali activator [55]. When the alkali activator contained soluble silicate compared to the only use of alkaline hydroxides, the higher rate of geopolymerization reaction was found [55]. Compared to NaOH, KOH showed a greater level of alkalinity and therefore allowed higher rates of silicate dissolution. The size of the cation was reported to affect the eventual crystal morphology, where K^+ provided higher degree of condensation as compared to Na^+ under the same conditions [49]. The smaller hydration sphere of K^+ than Na^+ allowed more dense and intimate polycondensation reactions and hence increased overall strength of the matrix [56].

Constituents effect. The SiO_2/Al_2O_3 ratio, R_2O/Al_2O_3 ratio, SiO_2/R_2O ratio (R=Na^+ or K^+) and liquid–solid ratio are the most important factors to affect the properties of geopolymer pastes [57,58]. The formation of crystalline zeolite ($Na_{96}Al_{96}Sr_{96}O_{384}216H_2O$) was reported when geopolymer activated with NaOH alone with Si/Na of 4/4 or less, whereas at a ratio >4/4 nanosized crystals of another zeolite ($Na_6[AlSiO_4]_6{\cdot}4H_2O$) were formed. The optimum

geopolymer strength was obtained with SiO_2/Al_2O_3 ratio in the range of 3.0–3.8 and Na_2O/Al_2O_3 ratio of ~1. Another study reported increase in the setting time of geopolymer pastes with increase in SiO_2/Al_2O_3 ratio [27]. The significance of SiO_2/R_2O ratio indicated the increase in compressive strength of geopolymers with increase in alkali content or decrease in silicate content [59].

Curing conditions. The number of studies has been devoted to the effect of different curing conditions on the properties of geopolymer pastes. The curing for longer periods of time at elevated temperature weakened the geopolymer structure due to substantial loss of moisture in geopolymers. This suggested that little amounts of structural water need to be retained to maintain structural integrity and eliminate cracking of geopolymers [60]. For fly ash based geopolymers, the prolonged curing at elevated temperatures destructed the gel structure of the geopolymer synthesis, resulting in excessive shrinkage and dehydration, while long precuring at room temperature was found beneficial for strength development. In another study, the curing of metakaoline-based geopolymers at ambient temperature was not feasible, while increase in temperature (40 °C, 60 °C, 80 °C, 100 °C) favored the strength gain after 1–3 days [61]. Similarly, another researcher reported that curing of metakaoline based geopolymer at elevated temperature (40–80 °C) accelerated the strength development, however realized deterioration in mechanical properties after 28 days in comparison with results obtained for an ambient temperature [62]. The later age failure of samples when cured at higher temperature for a longer period of time was attributed to the thermolysis of –Si–O–Al–O– bond. Almost all studies have mentioned adequate curing of geopolymeric materials to achieve optimal durability and mechanical performance [27].

C-S-H phase effect. The C-S-H phase effect has importance on the early age strength development of geopolymers. The strength of metakaoin/slag blends geopolymers was increased which was attributed to the presence of both aluminosilicate gel (N-A-S-H) and C-S-H phase [63]. Though, by addition of natural calcium silicate minerals at lower alkalinity, the little dissolution of calcium occurred to result in less C-S-H gel formation and less strength [64]. The hardening in fly ash/slag geopolymer combined with potassium silicate and potassium hydroxide was ascribed to C-S-H/C-A-S-H formation. Further, the effective increase in compressive strength was reported due to slower dissolution rate of calcium ions [65].

Effect of admixtures. The admixtures can act as retarders or accelerators for the geopolymerization reaction. The sucrose was reported to act as retarder as it was absorbed by Al, Fe and Ca ions to form insoluble metal complexes, whereas citric acid acted as an accelerator deceasing the setting time by 9 and 16 min, respectively [66]. The retarding effect of superplasticizer was studied in fly ash/slag blended system where polycarboxylate based superplasticizer showed significant improvement in workability compared to naphthalene based superplasticizer [27,67].

3.4 Elevated temperature properties of geopolymers

Effect of fibers. The benefits of geopolymers as ideal matrix for fiber-reinforced system in high-temperature applications have been investigated in number of previous studies. Various inorganic and organic fibers have been added into geopolymers to enhance its fire resistance e.g. PVA fibers, SiC fibers, basalt fibers, steel fibers, etc [68–71]. For instance Lyon et al. performed study on potassium aluminosilicate geopolymers at extended exposure to simulated fires and reported to retain 63% of the initial 245 MPa flexural strength after reinforcement with carbon fabrics [54]. On the other side, all other systems examined for comparative purposes (carbon- or

glass-fabric reinforced epoxy, polyimide, polyester, bismaleimide, vinyl ester, cyanate ester, phenolic, and engineering thermoplastics) ignited and began to produce heat and smoke in less than 30 min [72,73]. Similarly, Zhang et al. found excellent mechanical behavior of 2% carbon fiber reinforced geopolymer containing 50% fly-ash and 50% metakaoline at 500 °C [74]. Masi et al. reported better mechanical properties of basalt fiber reinforced geopolymer at elevated temperatures than its PVA fiber reinforced counterpart [43]. Alomayri et al researched on carbon and cotton fibers reinforced geopolymer composites at elevated temperatures [75]. Dylmar and Clelio investigated the impact of the volume percentage of the fibers on the rupture strength of geopolymer concretes reinforced with basalt fibers. Wang, and Zhou looked at the high-temperature behavior geopolymers with fiber loading of 20% by exposure 1000, 1100, 1200, 1300, and 1400 °C in an argon atmosphere for 90 min. They reported effective filling of oval pores, increase in relative density from 79% to 93%, increase in compressive strength by 35% at room temperature, and increase in flexural strength by up to 20% at elevated temperatures [76]. Zhao et al. examined stainless steel meshes constructed from 60 μm diameter fibers infiltrated by K_2SiO_3 activated quartz/corundum geopolymers. They reported that the addition of 10% of Al_2O_3 fibers did not show ductile behavior in pure geopolymers, but found enhancements in the flexural strengths of the samples that contained the stainless steel mesh [69]. The authors Kriven, Bell, and Gordon described soluble-silicate activated metakaoline geopolymer reinforced with chopped basalt fibers (10 μm diameter, 4 mm length) for use in glass refractories [77]. They found loss of workability by addition of 5% of basalt fiber. Pernica et al. used 70% and 55% of alkali-resistant glass and carbon fibers, respectively in a metakaoline geopolymer and found drop in composite stiffness and flexural strength by roughly 25% and 50%, respectively, when the tests were done above 150 °C [78].

Effect of fillers. Besides fibers, various granular fillers have been also used in geopolymer matrix to improve its fire resistance e.g. silica sand, calcite and dolomite sand, grinded electrical porcelain, grinded high-alumina refractory brick, α-Al2O3powder, α-quartz sand and fine alumina powder, chamotte powder, kyanite (nesosilicate) aggregates, cordierite powder, burned clay, expanded clay, quartz fume, etc [79–84]. The author Tie Song Lin et al. studied the effects of heat treatment temperatures up to 1200 ℃ on the thermal-mechanical properties of short carbon fiber preform reinforced geopolymer composites consisting of different contents of α-Al_2O_3 fillers [85]. They found no improvement in the mechanical properties of composites at room temperature, however certain improvements at high temperature by addition of α-Al_2O_3 particles. The minimum values of flexural strength and fracture work of the composites was observed in the temperature range of 600−800 ℃(See Figure 8).

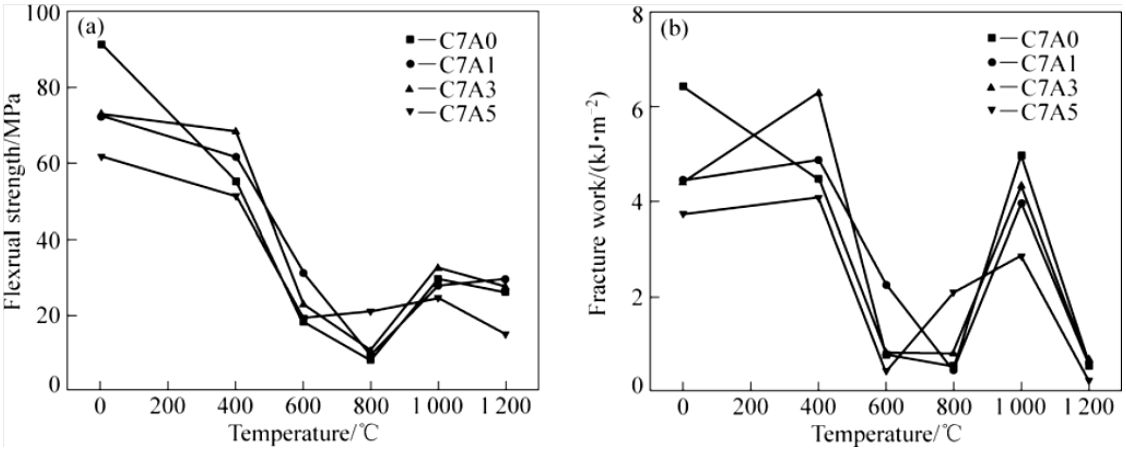

Figure 8. Flexural strength (a) and fracture work (b) of α-Al_2O_3/geopolymer composites after exposure to different temperatures [85].

In other study, Bernal et al. investigated the mechanical performance of metakaoline-based geopolymers reinforced with refractory aluminosilicate particles and fibers after exposure to elevated temperatures (Figure 9). The addition of refractory particles, without as well as with additional refractory fibers, was found to promote the enhanced post-exposure compressive

strength at 600 °C and 1000 °C. The incorporation of fibers contributed further to the enhancement of the residual compressive strength after exposure to high temperatures. On the contrary, 84% reduction in the compressive strength was observed for the specimens of neat geopolymers when exposed to elevated temperatures [86].

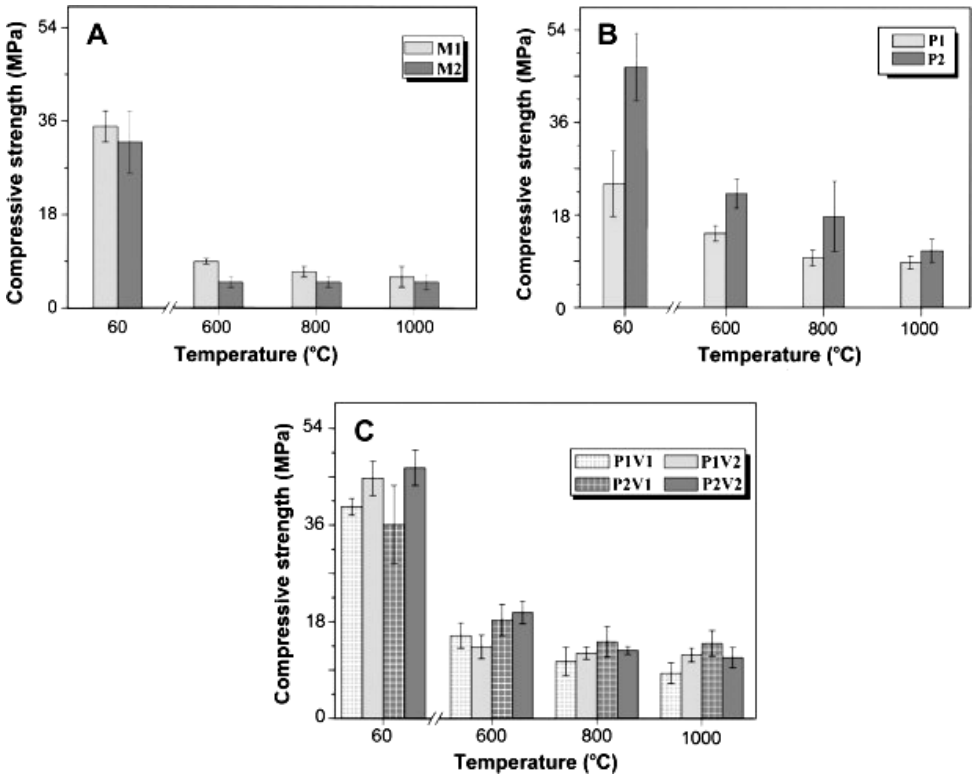

Figure 9. Compressive strengths of (a) unreinforced geopolymer matrices, (b) particle reinforced and (c) particle-fiber reinforced geopolymer composites [86].

Hemra and Aungkavattana (2016) studied the compressive strength of cordierite-metakaoline based geopolymer composites and reported to reach 15 cycles of thermal shock test without cracking of geopolymer composites when 50 wt% cordierite were added (Figure 10) [84],

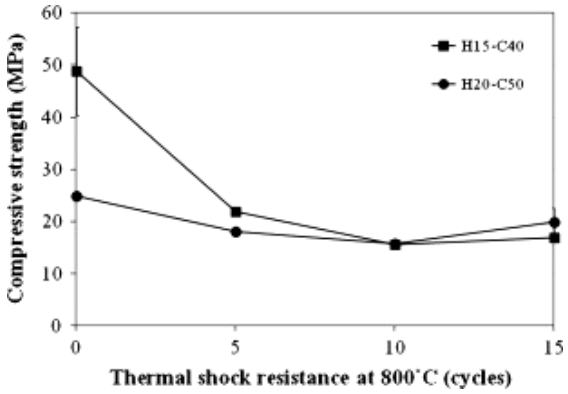

Figure 10. Compressive strength of cordierite/geopolymer composites at 800 °C [84]

Another study investigated the possibility of using 0% to 30% quartz powder to upgrade the compressive strength as well as the workability of alkali-activated metakaoline paste before and after treatment to elevated temperatures (Figure 11). They reported 1.04 folds enhancement in residual compressive strength value at 400 °C, 600 °C, 800 °C and 1000 °C by addition of only 5% quartz powder, whereas 1.21 folds for 30% quartz powder content [87].

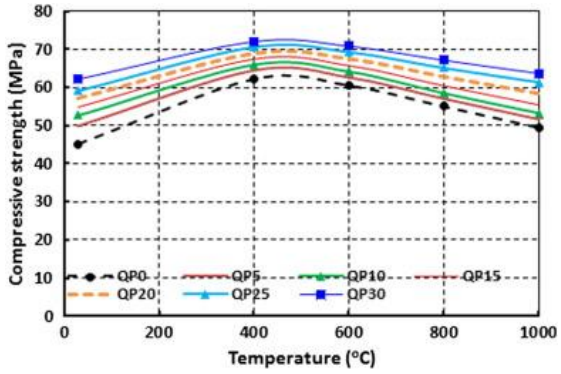

Figure 11. Compressive strength of quartz powder/geopolymer composites [11,87].

Figure 12 presented another study on geopolymer binders made from metakaoline and fly ash blend. It showed highest bending and compressive strength after exposure to 500 °C for the specimens of 50% metakaoline and 50% fly ash [88].

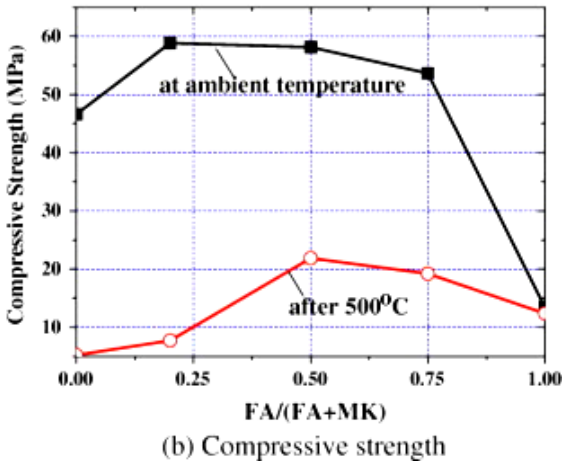

Figure 12. Effect of fly ash content on compressive strength of geopolymer pastes [87].

In Figure 13, the study investigated the thermo mechanical behavior of geopolymer matrices composed by metakaoline, silica fume and blast furnace slag. Utilization of various aggregates was studied by substitution natural sand with chamotte. The presence of blast furnace slag in the geopolymer mixture considerably increased its mechanical response, whereas the incorporation of silica fume showed inferior performance. Furthermore, the substitution of sand with chamotte resulted in better compatibility above 500ºC. In aggressive temperature environments, the chamotte reinforced matrix showed that the greatest mechanical performance achieving 19.82 MPa at 1000 ºC [89].

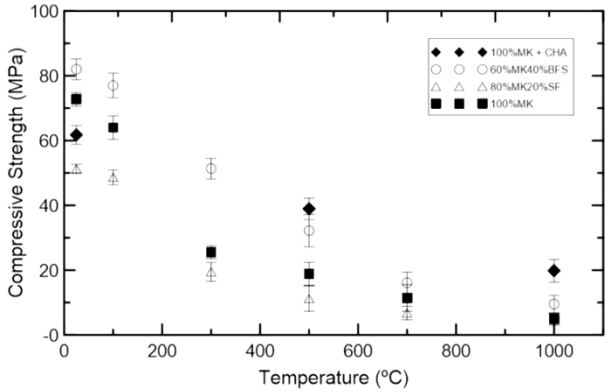

Figure 13. Compressive strength of the metakaoline geopolymers after addition of silica fume, blast furnace slag and chamotte [89].

4 CHAPTER: RESEARCH METHODOLOGY

4.1 Materials

The recycled carbon materials under trade name carbiso mil 100 μ were purchased from Easy composites, UK, whereas the short basalt fibrous waste was obtained from the VEBA Industries, Czech Republic. The basalt fibers had density of 2650 kg/m^3, initial modulus of 95 GPa, tensile strength of 4 GPa, elongation at break of 3 % and water absorption of less than 0.5 %. The chemical composition of basalt fibers as measured from elemental analysis is shown in Table 3.

Table 3.Elemental analysis of basalt fibers

Element	Oxygen	Sodium	Magnesium	Aluminum	Silicon	Potassium	Calcium	Iron
Weight %	42.41	0.56	1.04	5.39	14.79	0.97	5.72	10.27

The Baucis L110 alumino-silicate geopolymer binder based on metakaolin was obtained from Ceske Lupkove Zavody, Czech Republic along with sodium alkali activator. The metakaolin geopolymer was synthesized from calcined kaolin and shale clay residues with Si/Al ratio of 2.0. The kaolin was mainly composed of kaolinite with small amounts of quartz, whereas shale clay was composed of kaolinite with low amount of quartz and anatase. At first, kaolin and shale clay were passed in rotary klin to result in 30-70% loss of kaolinitic structure due to dehydroxylation. Later, it was converted to metakaolin by additional calcinations at 750 ^{o}C for 10 h in bath oven. The chemical composition of the metakaolin geopolymer was as follows (wt.%): SiO_2 47, Al_2O_3 24, LOI 0.5, Fe_2O_3 0.50, TiO_2 0.8, MgO 3.5, K_2O 0.40, CaO 17.50. The mean particle size (d50) was 5 μm. The sodium alkali activator was mixture of Na_2SiO_3 and NaOH.

4.2 Geopolymerization of metakaoline

Kaolinite has 1:1 uncharged dioctahedral layer structure with a chemical formula of $Al_2O_3 \cdot 2SiO_2 \cdot 2H_2O$ [90]. This layer comprises of $(Si_2O_5)_n^{2-}$ sheet and the $Al(OH)_3$ (gibbsite) sheet linked together by sharing oxygen atoms by van der Waals and hydrogen bonds as shown in Figure 14 [90]. As the near zero charges restricted the exchange of ion when attacked with alkali reactant, the chemical attack of kaolinite layers started from the surface edge and slowly penetrated inside the structure layer by layer (see Figure 15) [19]. This becomes the main factor that causes the low strength performance of most clay-based geopolymers. Therefore, metakaolin rather than kaolinite as a starting material is advantageous (i.e. high reactivity and purity) to have better compressive strength, high surface area, and voluminous porous surfaces of geopolymers. From Figure 16, the formation of Al-substituted silicate layers in metakaoline can be seen after the attack by NaOH solution [91].

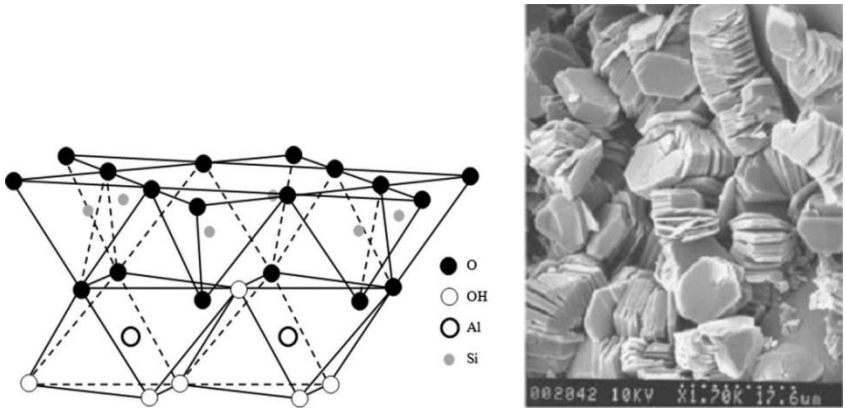

Figure 14. (a) Structure of kaolinite and (b) microstructure of kaolinite [92].

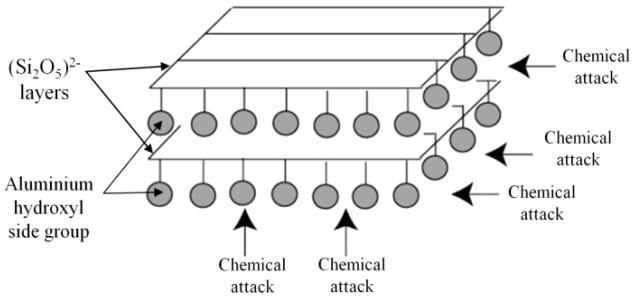

Figure 15. Chemical attack of kaolinite layers [19].

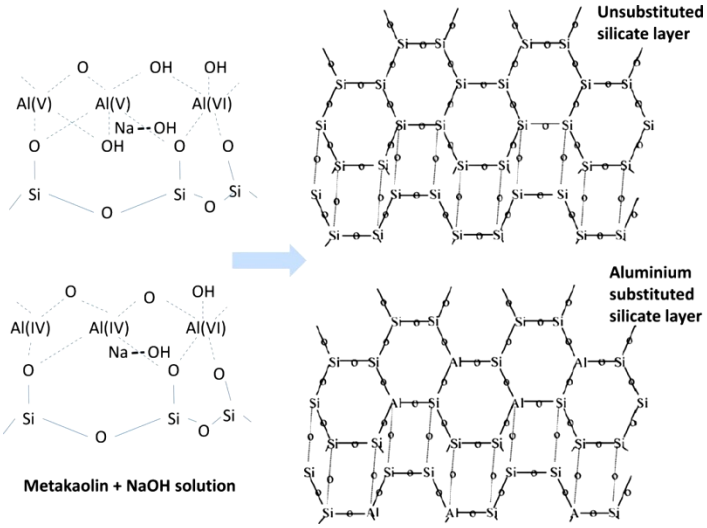

Figure 16. Geopolymerization of metakaolin with NaOH solution [93].

4.3 Preparation of carbon and basalt micro fibers

The short basalt fibrous waste was dipped in acetone for 24 h to remove the surface finish and impurities. For preparation of carbon and basalt microfibers, 30 min dry grinding was carried out by high-energy planetary ball mill of Fritsch Pulverisette 7, Germany in a sintered corundum container of 80 ml capacity using zirconium balls of 10 mm diameter [94,95]. The ball to material ratio was kept at 10:1 and the speed was kept at 850 rpm. Later, Malvern zetasizer nano series based on dynamic light scattering principle of Brownian motion of particles was employed to characterize the particle size distribution of dry milled carbon/basalt particles. Deionized water was used as dispersion medium and it was ultrasonicated for 5 min with bandelin ultrasonic probe before characterization. In addition, microstructure of milled particles was

observed on scanning electron microscope (SEM) of Hitachi–model TM-3000 at accelerated voltage of 15 kV.

4.4 Preparation of geopolymer composites

The four parts of sodium alkali activator and five parts of metakaoline based geopolymer were manually mixed for 10 min to ensure homogeneous preparation of geopolymer binders. For preparation of geopolymer composites, the carbon and basalt microfibers were initially pre-dried for 60 min at 70 ^{o}C in an oven. Next, both carbon/basalt micro fibers were added into the prepared geopolymer binder separately at 5 wt %, 10 wt % and 15 wt % loading. The mixing was homogeneously done in Hobart mixer for 5 min. Subsequently, the fresh prepared composite mortar was poured into 40 mm cubic-shaped moulds, vibrated for 2 minutes on the vibration table to remove air voids and wrapped using a thin plastic sheet to prevent water evaporation. The wrapped samples were demolded after 24 h of casting and then cured at room temperature (20 ± 2 ^{o}C) and a relative humidity of (70 ± 10 %) for 28 days.

4.5 Exposure to elevated temperature

The prepared geopolymer composites were exposed to elevated temperatures of 200, 400 and 800 ^{o}C at age of 28 days. The specimens were placed into a furnace (Elektrické Pece Svoboda, Czech Republic) and heated at fixed heating rate of 5 ^{o}C/min. As soon as the target temperature was attained, it was maintained for an additional 60 min. The furnace was then shut down to allow the specimens in the furnace to cool down to room temperature. Meanwhile, the unexposed specimens were left undisturbed at ambient condition.

4.6 Microstructure of geopolymer composites

The low vacuum scanning electron microscopy (SEM) of Hitachi–model TM-3000, coupled with X-rays microanalysis system of energy dispersive spectroscopy was employed to investigate the microstructure of geopolymer composites. It was carried out at 15 kV accelerated voltage. The samples were directly observed under the SEM without metallic coating due to low vacuum operations. The images were formed by acquisition of backscattered electrons at different magnifications.

4.7 Image analysis of geopolymer composites

It was employed to perform the pore area analysis on SEM images using IMAGEJ software. At first, the quality of images was improved by contrast enhancement and noise removal. Then, the images were segmented by proper thresholding method. In the current study, Otsu thresholding was suitably used to transform the images into binary form. The benefit of acquiring binary image is that it diminishes the difficulty of the data and simplifies the process of recognition and classification of porous and non porous area. Accordingly, the pore area (%) was evaluated by IMAGEJ software. Pore area (%) comprises the measurement of individual pore, summing up of all the individual pores and dividing the sum by the total area of the image [96].

4.8 Phase composition of geopolymer composites

The X-ray diffraction (XRD) test was performed to investigate the phase composition of geopolymer composites when exposed to the elevated temperatures. The samples were prepared into powder form by cutting small geopolymer slices. The test was carried out using PANalytical X'pert PRO equipment in 2 h-range of 5 to 80 θ at operating conditions of 40 kV and 30 mA using a Cu ka X- ray source.

4.9 Physical properties of geopolymer composites

The hardness of geopolymer composites was measured on the Rockwell H scale using an Avery Rockwell hardness tester. The samples were polished with emery paper to achieve flat and smooth surfaces before the measurement. The test was repeated for 5 samples. The average of measurements and 95% confidence interval limits were taken. Furthermore, the values of bulk density was determined in accordance with the ASTM-C948 2014 using the Eq. (1) [97]. The test was repeated for 5 samples and an average of measurements was taken.

$$\text{Bulk density} = \frac{W_d}{W_a - W_i} \times \rho \qquad (1)$$

Where W_d is dry specimen's mass after 24 h at 105 °C, W_i is specimen's mass immersed in water, W_a is saturated specimen's mass with a dry surface and ρ is the bulk density of water (kg m^{-3}). The average of measurements and 95% confidence interval limits were taken for measurements of 5 readings.

4.10 Compression strength of geopolymer composites

The geopolymer composites were tested for compression testing using Labor Tech universal testing machine, Czech Republic with load cell capacity of 2000 kN. The 40 mm cubes were tested for the determination of compression strength according to ASTM C109 standard. The test was repeated for 5 samples. The average of measurements and 95% confidence interval limits were taken.

4.11 Thermal stability of geopolymer composites

The thermo gravimetric analysis (TGA) was performed to know the thermal stability of geopolymer composites from weight loss with increase in temperature. It was conducted using TGA/SDTA 851 METLER TOLEDO analyzer. Samples with 10 mg were placed in an alumina

crucible and tests were carried out in air atmosphere with a heating rate of 10 °C/min from 30 to 1000 °C.

5 CHAPTER: RESULTS AND DISCUSSIONS

5.1 Characterization of carbon and basalt micro fibers

Figure 17 (a) shows the particle size distribution results of basalt particles obtained after 30 min of dry milling. It can be observed that short basalt fibrous waste was transformed into basalt particles of micro to nano scale in multimodal distribution. With longer milling time, the basalt particles were found to deposit onto the walls of milling containers. This behavior was attributed to increase in temperature of ball mill and following cold welding of basalt particles on milling container [94]. For more homogeneous refinement of basalt particles to nano scale, it is essential to pulverize them for prolonged duration by overcoming the rise in temperature of ball mill. Figure 17 (b) showed the SEM image of microstructure of basalt particles after 30 min of dry milling. The shape of basalt particles was observed largely in the form of microfibrils with few particles below 10 µ scale.

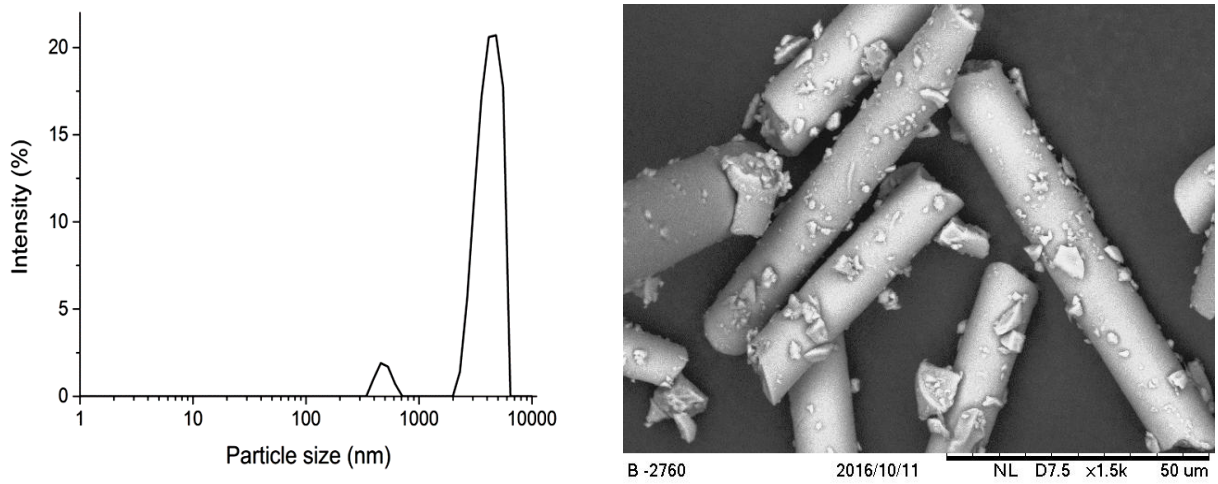

Figure 17. (a)Particle size distribution of basalt particles after 30 min dry milling (b). SEM image of basalt fibers after 30 min dry milling

Likewise, for uniform dispersion of carbiso mil 100 µ particles in geopolymer system, their surface was mechanically activated using 30 min dry pulverization. Figure 18 shows the particle size distribution results of carbiso mil 100 µ particles after dry milling. It can be seen that carbiso mil 100 µ particles were converted into fine carbon micro structures having multimodal distribution after 30 min dry milling. Further, the morphology of carbon particles was investigated with the help of SEM images shown in Figure 19. The shape of carbon particles was observed predominantly in the form of microfibers with few of microparticles below 10 µ scale. Unlike basalt particles, the deposition of carbon particles was found less severe with longer milling time. Therefore, the relative percentage of CMF or microparticles can be altered based on the duration of the milling action. The shorter milling time can produce more of microfibers and longer milling time can produce more of microparticles. The milling time of 30 min was fixed in this study because of the requirement of higher aspect ratio of CMF for effective reinforcement in composites.

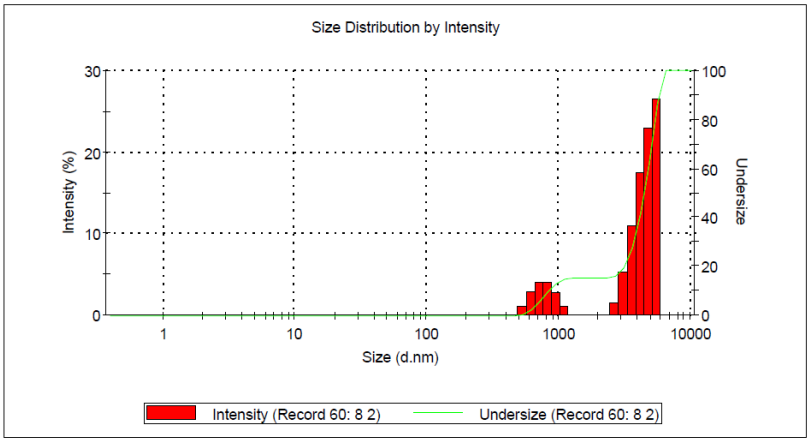

Figure 18. Particle size distribution of carbiso particles after 30 min dry milling

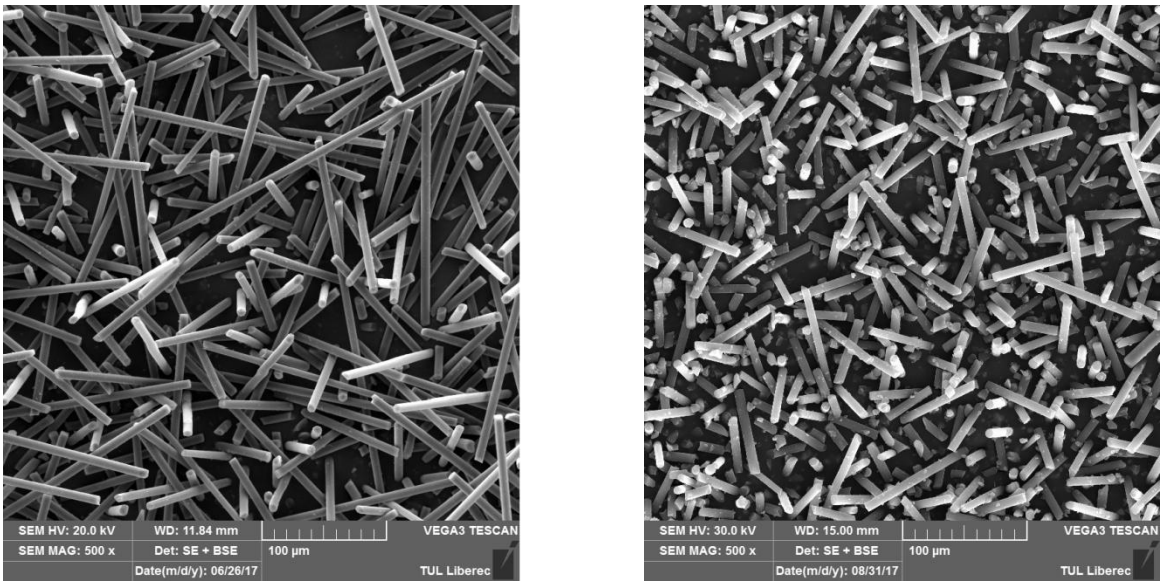

(a) before milling (b) after milling

Figure 19. Microstructure of carbiso powder

5.2 Microstructure analysis of geopolymer composites

The SEM micrographs of the neat geopolymer and BMF/geopolymer composites before and after exposure to the elevated temperatures are shown in Figure 20. The typical microstructure of homogeneous and dense matrix consisting mostly of alumino-silicate gel was viewed before exposure to the elevated temperatures. The micrographs of geopolymer composites demonstrated the smooth surfaces of BMF in the geopolymer matrix, which pointed out no degradation of basalt fibers owing to action of alkali in the activating solution. The BMF appeared to have reacted with the geopolymer matrix to some extent. The majority of the microfibrils were covered by the geopolymer, which pointed out possible physical bonding of geopolymer matrix with basalt fibers. In addition, the geopolymer composites exposed the chances of ductile failure from observations of indistinct cross-sections of basalt fiber ends. When the samples exposed to elevated temperatures, the development of higher bright crystals

content, wider micro- cracks, and the relatively large voids were noticed. The compact microstructure of geopolymers became more porous at 800 ^{o}C, which might be caused by weight loss, matrix decomposition and phase transformations [43,98]. The geopolymer composites revealed lesser microstructural deterioration at elevated temperatures than neat geopolymers and hence eventual less strength loss. This showed the formation of dense microstructure by BMF, which gave resistance to the penetration of heat. This can be attributed to the mechanical percolation along with pore filling effects of BMF at elevated temperatures [99,100]. Further, the thermal resistance characteristics of BMF were identified from appearance of fibers in micrographs of samples exposed to 800 ^{o}C. The loose interface layer attributable to enlarged space between the matrix and microfibrils resulted in the strength reduction of geopolymer composites at increased temperature [101].

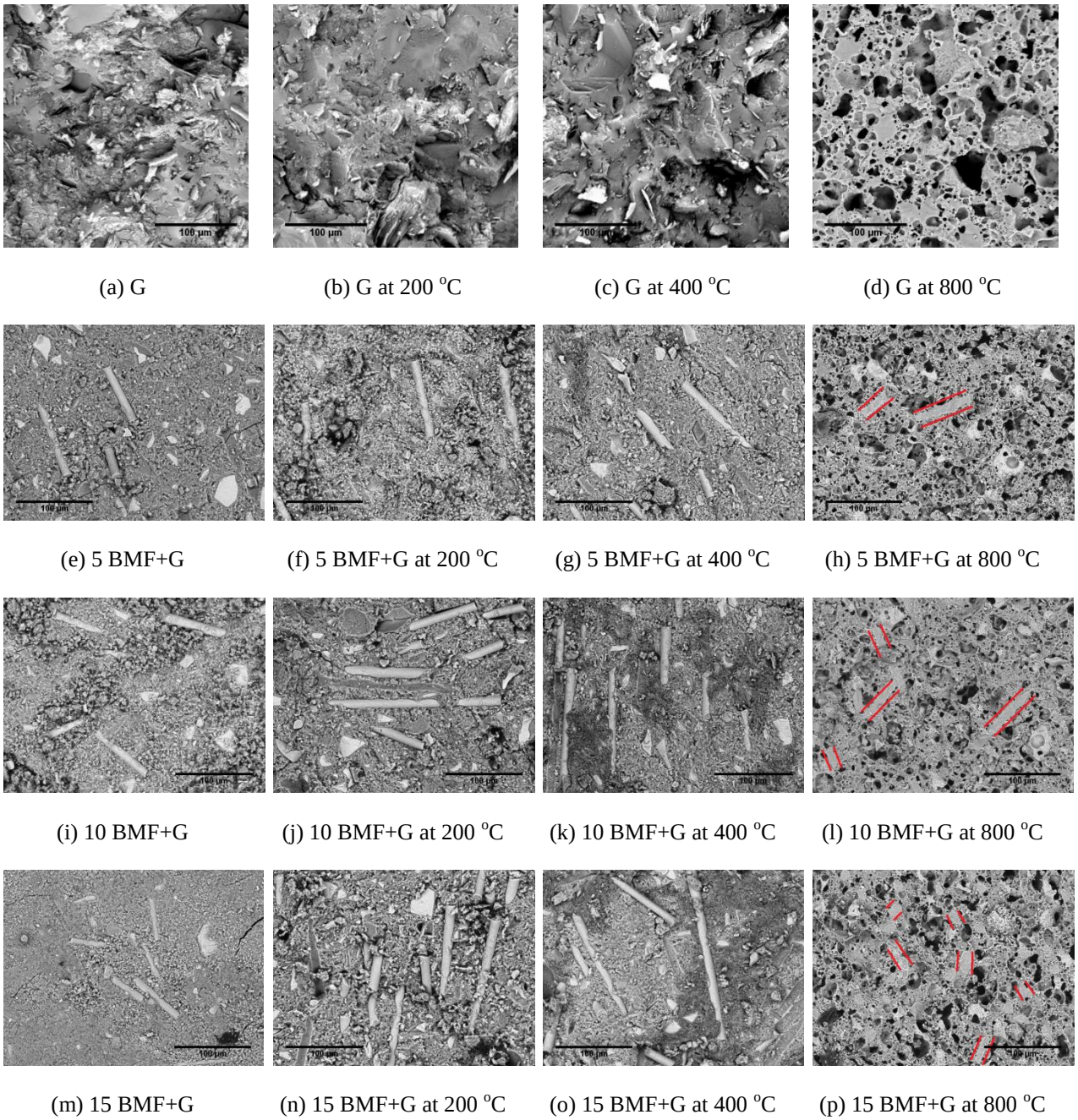

(a) G (b) G at 200 °C (c) G at 400 °C (d) G at 800 °C

(e) 5 BMF+G (f) 5 BMF+G at 200 °C (g) 5 BMF+G at 400 °C (h) 5 BMF+G at 800 °C

(i) 10 BMF+G (j) 10 BMF+G at 200 °C (k) 10 BMF+G at 400 °C (l) 10 BMF+G at 800 °C

(m) 15 BMF+G (n) 15 BMF+G at 200 °C (o) 15 BMF+G at 400 °C (p) 15 BMF+G at 800 °C

Figure 20. Microstructure of basalt microfibril/geopolymer composites at elevated temperature

The SEM micrographs of neat geopolymer and CMF/geopolymer composites at different temperature exposure are shown in Figure 21. The smooth surfaces of carbon fibers in the geopolymer matrix indicated no degradation of carbon fibers under action of alkali in the activating solution. The strong adhesion between the geopolymer gel and the surface of the fiber

can be confirmed based on presence of geopolymer layer on fiber ends pulled out from the matrix and more striations on fiber surfaces [43]. Furthermore, the fractured surfaces of neat geopolymer showed straight cracks, whereas more number of curvilinear small cracks was found in case of geopolymer composites due to crack deflections by CMF. Therefore, it can be concluded that the addition of CMF ensured the effective toughening mechanism to prevent the catastrophic fracture of geopolymers. When the samples exposed to elevated temperatures, the geopolymer composites showed lower micro structural deterioration than neat geopolymers due to possible mechanical percolation along with pore filling effects of carbon micro fibers [99,100]. This observation was further investigated by image analysis. The development of wider micro- cracks, higher bright crystals content and the relatively large voids were observed with increased temperature exposure. As discussed previously, this might be caused by weight loss, matrix decomposition and phase transformations in geopolymers at higher temperature [43,98]. The CMF did not exhibit any observable degradation after elevated temperature exposure. However, previous studies highlighted the significant degradation of polymeric fibers, glass fibers, basalt fibers, etc after such temperature exposure [75]. This indicated the thermal resistance characteristics of CMF that can continue to provide the reinforcement to geopolymers when exposed to higher temperatures and therefore less strength loss. Nevertheless, the development of loose interface layer caused by enlarged space between fibers and the matrix at elevated temperatures can possibly reduce the strength of geopolymers to some extent [101].

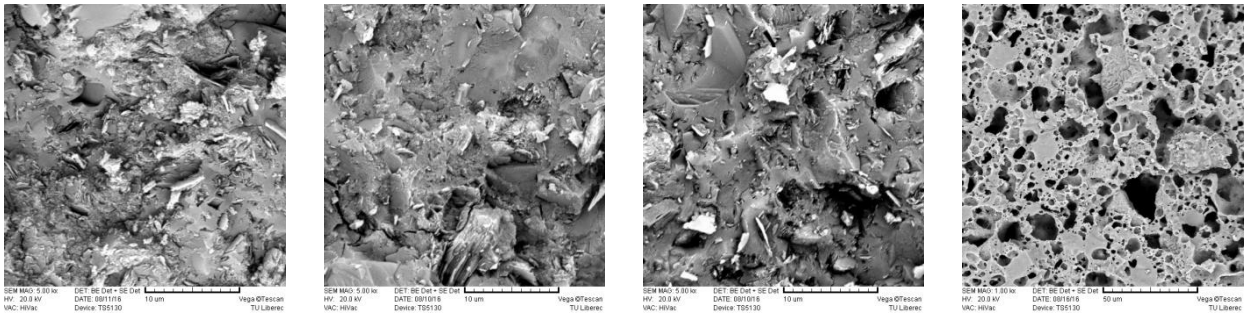

G | G at 200 ^{o}C | G at 400 ^{o}C | G at 800 ^{o}C

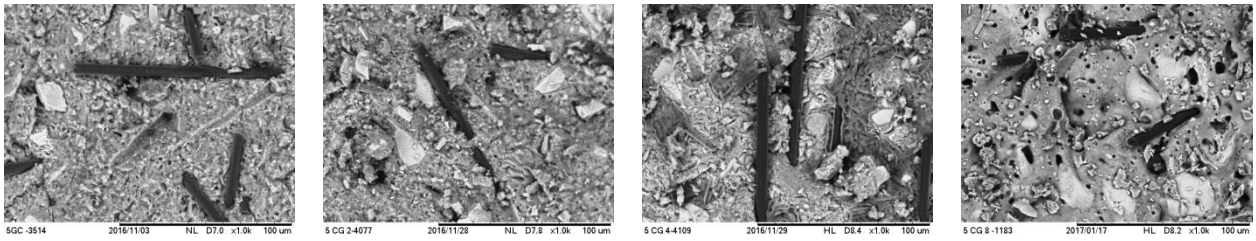

5 CMF+G | 5 CMF+G at 200 ^{o}C | 5 CMF+G at 400 ^{o}C | 5 CMF+G at 800 ^{o}C

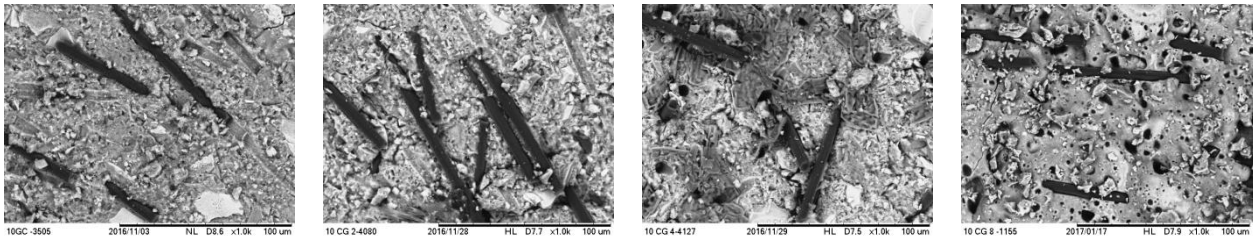

10 CMF+G | 10 CMF+G at 200 ^{o}C | 10 CMF+G at 400 ^{o}C | 10 CMF+G at 800 ^{o}C

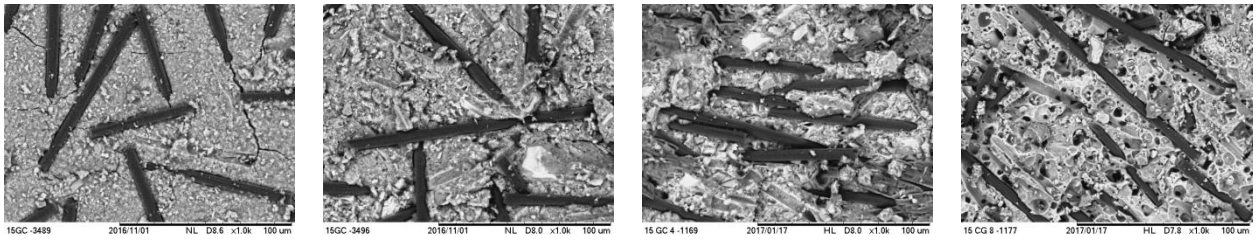

15 CMF+G | 15 CMF+G at 200 ^{o}C | 15 CMF+G at 400 ^{o}C | 15 CMF+G at 800 ^{o}C

Figure 21. Typical fracture surface microstructure of carbon microfiber/geopolymer composites after exposure to elevated temperature

5.3 Image analysis of geopolymer composites

The quantitative analysis of the pore area is important to establish the relationships between microstructure and mechanical properties of geopolymer composites after exposure to elevated temperatures. In present work, image analysis was used for estimation of pore area analysis by observation of large capillary pores and voids in binary images of Figure 22 and Figure 23. At first, SEM images were carefully converted into binary images by segmentation of Otsu thresholding method. The pore area was represented by black color in binary images and it was calculated in pixels by IMAGEJ software. Such 20 images of each sample were analyzed and average of pore area was determined (see Figure 24(a) and 24(b)). The pore area was found to reduce with increase in loading of BMF or CMF, which supported the previous observation of pore filling ability. However, the BMF/geopolymer composites depicted greater pore area than CMF/geopolymer composites across all range of to elevated temperature exposures. This indicated greater pore filling ability of CMF than BMF due to their thermal resistance properties across all elevated temperatures. Therefore, the higher mechanical properties were expected from geopolymers filled with CMF as compared to BMF.

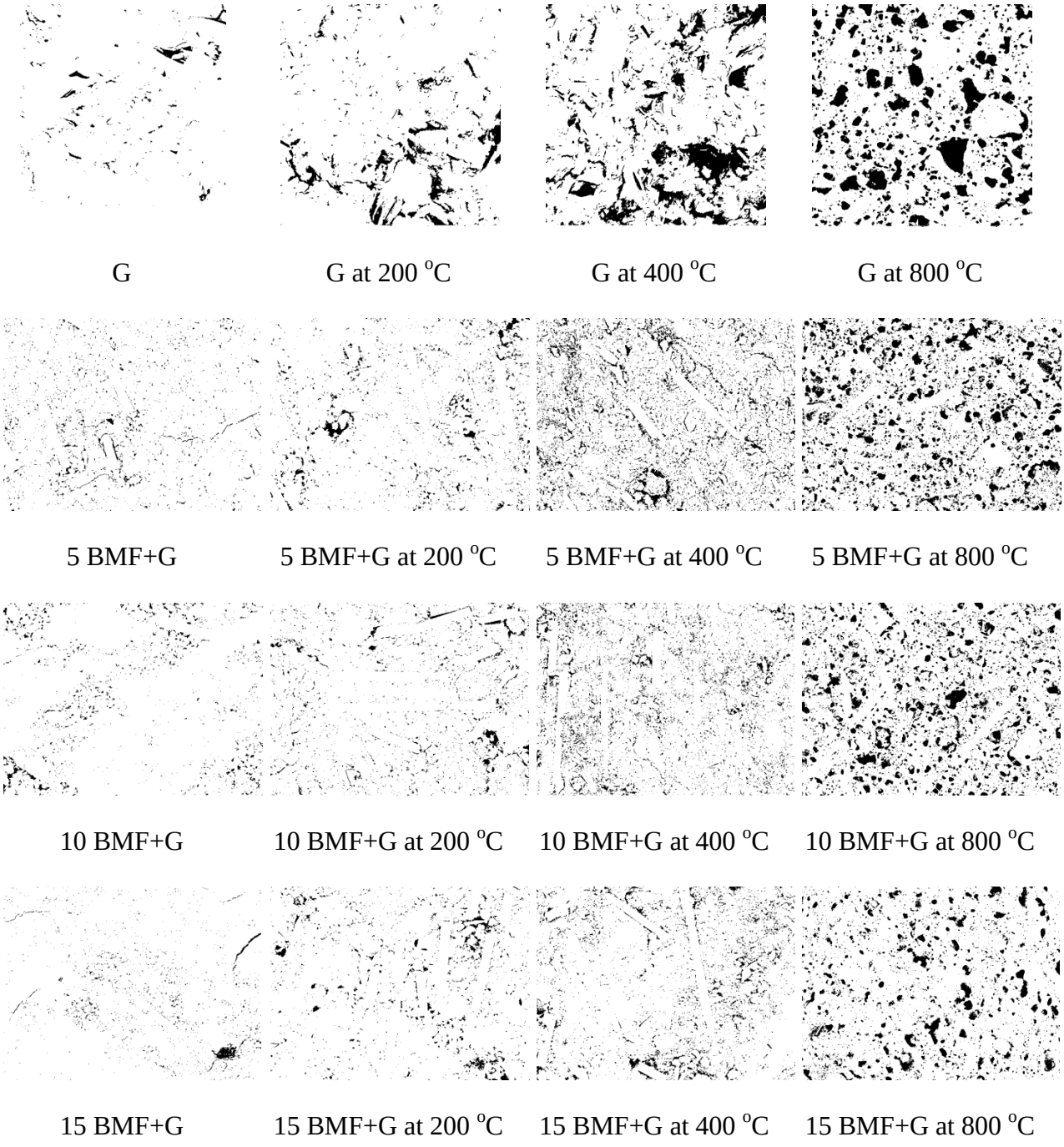

Figure 22. Estimation of pore area in basalt microfibril/geopolymer composites by image analysis

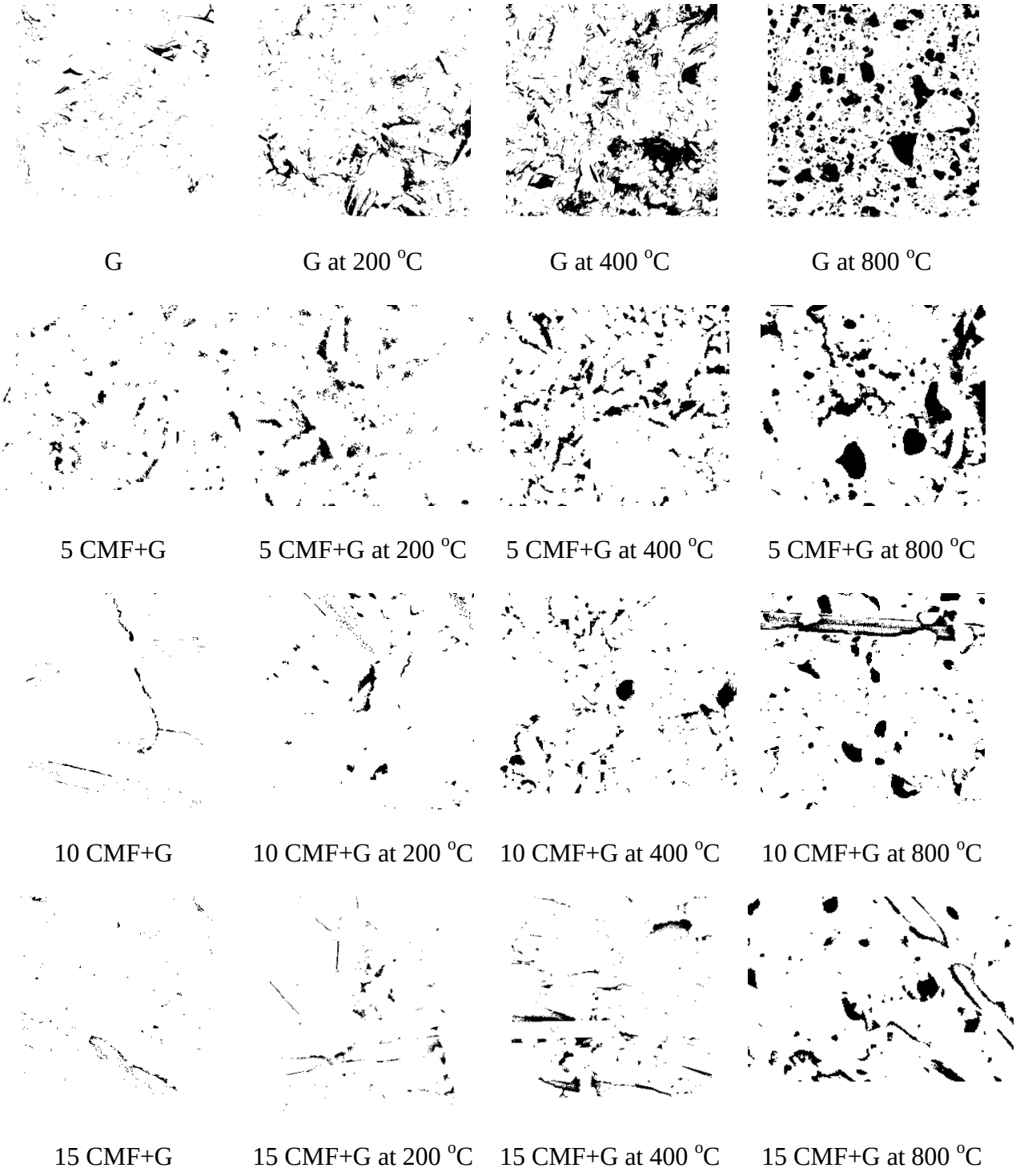

Figure 23. Estimation of pore area in carbon microfiber/geopolymer composites by image analysis

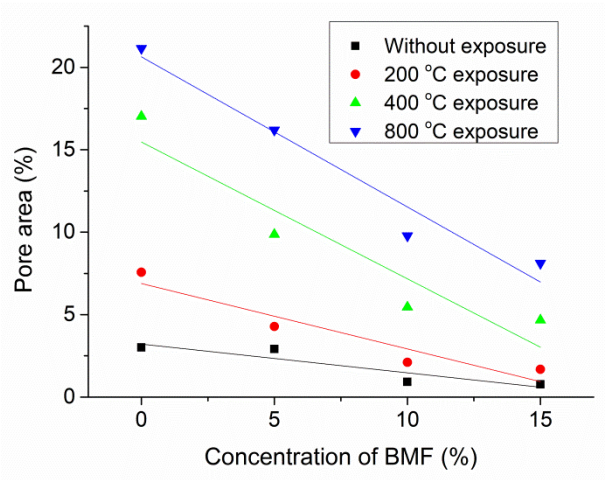

(a) BMF/geopolymer composites

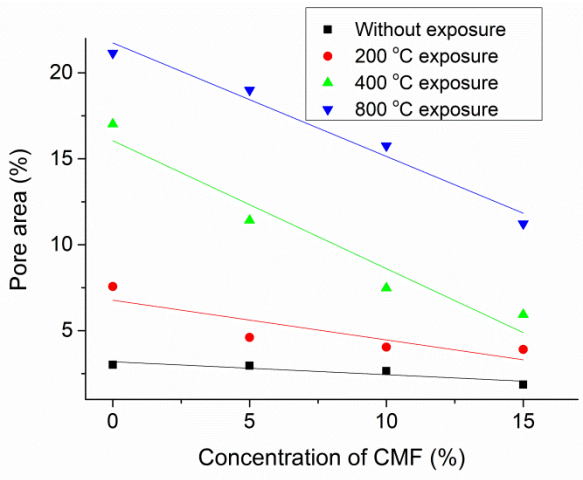

(b) CMF/geopolymer composites

Figure 24. Estimation of pore area of geopolymer composites

Further, the sensitivity in pore area changes after addition of BMF or CMF in geopolymers was estimated by using method of least squares for linear regression Equation (2).

$$Pore\ area = a + (b \times temperature) \qquad (2)$$

Table 4 shows the calculated parameters where slope indicates the sensitivity in changes of pore area. As compared to CMF/geopolymer composites, the slope of BMF/geopolymer composites was found to change significantly. This indicated better stability of CMF/geopolymer composites and greater thermal resistance of CMF than BMF. Further, the sensitivity in changes of pore area was found less at lower concentration of fillers, however it increased with increased concentration of BMF or CMF.

Table 4.Estimation of sensitivity of pore area changes by linear regression method

	Sample	Intercept	Slope	R^2
BMF geopolymer composites	Without exposure	3.20±0.49	-0.17±0.05	0.76
	200 ^{o}C exposure	6.88±0.84	-0.39±0.09	0.85
	400 ^{o}C exposure	15.47±1.88	-0.82±0.20	0.84
	800 ^{o}C exposure	20.63±1.27	-0.91±0.13	0.93
CMF geopolymer composites	Without exposure	3.18±0.22	-0.07±0.02	0.75
	200 ^{o}C exposure	6.76±0.87	-0.23±0.09	0.62
	400 ^{o}C exposure	16.04±1.20	-0.74±0.12	0.91
	800 ^{o}C exposure	21.73±0.70	-0.66±0.07	0.96

5.4 Physical observations of geopolymer composites

Figure 25 illustrates photographs of the physical observation of the neat geopolymers and BMF/geopolymer composites when exposed to the elevated temperatures of 200, 400, and 800 ^{o}C, respectively. The increased amount, width and length of thermal cracks were found for neat geopolymers than BMF/geopolymer composites. The cracks further increased with increasing the elevated temperatures. The dehydration/dehydroxylation of the geopolymers, subsequent decomposition of dehydrated aluminosilicates and the volumetric expansion of unreacted phases were considered as responsible factors for development of cracks at higher temperature exposure [102].

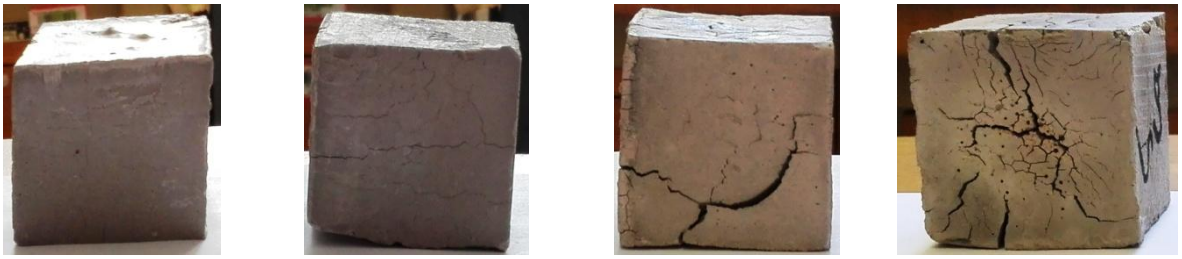

(a) G (b) G at 200 °C (c) G at 400 °C (d) G at 800 °C

(e) 5 BMF+G (f) 5 BMF+G at 200 °C (g) 5 BMF+G at 400 °C (h) 5 BMF+G at 800 °C

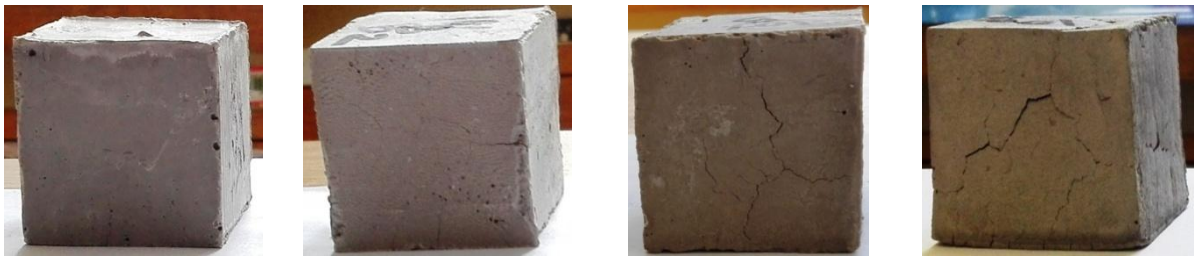

(i) 10 BMF+G (j) 10 BMF+G at 200 °C (k) 10 BMF+G at 400 °C (l) 10 BMF+G at 800 °C

(m) 15 BMF+G (n) 15 BMF+G at 200 °C (o) 15 BMF+G at 400 °C (p) 15 BMF+G at 800 °C

Figure 25. Basalt microfibril/geopolymer composites at elevated temperature

On the contrary, the CMF/geopolymer composites showed intact original structural characteristics with minimum development of thermal cracks in comparison to BMF/geopolymer composites (see Figure 26). The relatively higher thermal durability of CMF/geopolymer

composites was attributed to the presence of high thermal resistant thin CMF which bridged the cracks when exposed to the elevated temperatures [103].

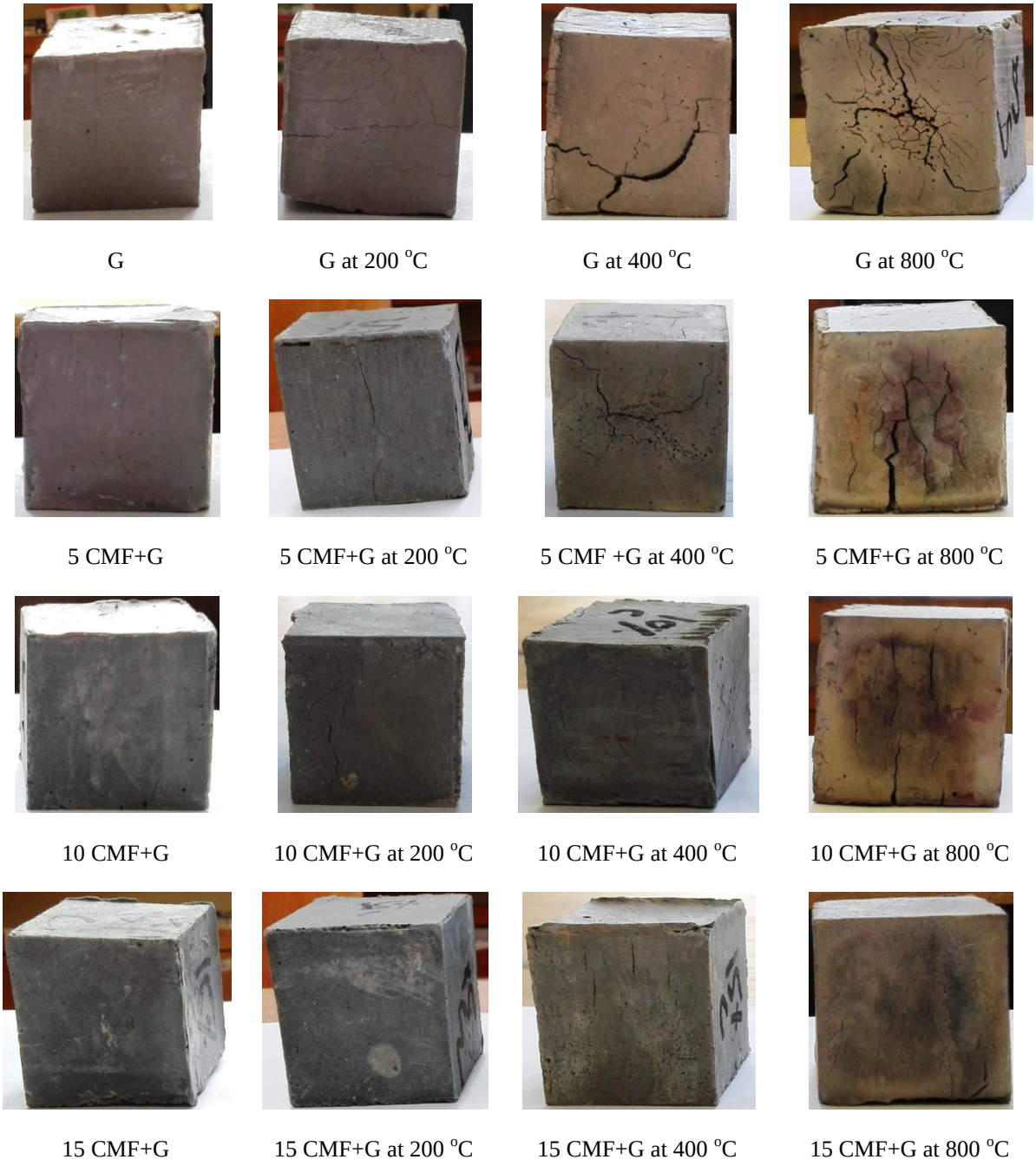

Figure 26. Carbon microfibril/geopolymer composites after exposure to elevated temperature

5.5 Elemental analysis of geopolymer composites

Table 5 shows the identified elements in the BMF-geopolymer composites. All samples exhibited high concentrations of silicon, oxygen and aluminum, which indicated the formation of alumino-silicate gels. The most important factors affecting the formation of alumino-silicate gels are SiO_2/Al_2O_3 ratio, Na_2O/Al_2O_3 ratio, SiO_2/Na_2O ratio and liquid–solid ratio. An increase in alkali content or decrease in silicate content increases the formation of aluminosilicate network structure [104]. Additionally, the high concentrations of calcium and sodium after incorporation of BMF were found in geopolymer composites. This indicated the formation of additional calcium silicate or calcium alumino-silicate and sodium alumino-silicate hydrates from inorganic contents in basalt fibers [102]. The extra precipitation of calcium alumina silicate hydrates formation can be attributed to nucleating sites present on BMF. The Si/Al molar ratio was increased till 400 ^oC and then dramatically reduced at 800 ^oC. The increased silicate portion was believed to be responsible for the densification and sintering processes in the geopolymer paste [99]. Therefore, the formation of thermally stable, more compact and dense microstructures of geopolymers can be concluded due to filling of BMF.

Table 5. Elemental analysis of basalt microfibril/geopolymer composites at elevated temperature

Element	Weight (%)												
	G	5 BG	5 BG 2	5 BG 4	5 BG 8	10 BG	10 BG 2	10 BG 4	10 BG 8	15 BG	15 BG 2	15 BG 4	15 BG 8
Carbon	-	5.14	3.43	-	2.67	-	-	4.43	4.51	-	-	-	0.35
Oxygen	58.02	59.38	46.52	54.62	53.92	52.16	61.94	55.51	56.84	54.98	49.45	50.90	58.23
Sodium	4.06	6.16	4.61	2.48	7.08	4.61	2.90	7.70	4.64	3.57	5.64	6.47	2.72
Magnesium	0.55	0.79	0.97	3.50	0.75	0.82	1.78	0.89	0.78	1.46	0.54	0.70	3.84
Aluminum	9.24	7.47	5.25	4.22	12.23	10.67	7.38	7.85	6.44	8.27	10.30	10.61	6.10
Silicon	22.58	17.50	19.48	15.27	18.17	26.13	18.56	19.97	17.81	22.13	25.71	24.64	15.83
Sulphur	-	-	-	0.40	-	0.49	-	-		-	-	-	0.30
Potassium	0.44	-	0.30	0.56	0.66	-	0.74	-	0.80	0.57	0.69	1.20	0.31
Calcium	5.06	3.52	19.41	18.90	3.85	5.08	3.36	3.62	8.14	5.58	6.65	5.46	12.28
Titanium	-	-	-	-	-	-	0.38	-	-	0.48	0.97	-	-
Iron	-	-	-	-	0.64	-	2.92	-	-	2.93	-	-	-

Table 6 shows the identified elements in the CMF-geopolymer composites. Likewise in previous discussion, all samples exhibited high concentrations of silicon, oxygen and aluminum, which indicated the formation of alumino-silicate gels. Additionally, the high concentrations of calcium and sodium with increase in carbon microfiber loading were found in geopolymer composites. This indicated the formation of additional calcium silicate or calcium alumino-silicate and sodium alumino-silicate hydrates. The Si/Al molar ratio was found to increase with increase in temperature. The increased silicate portion was believed to be responsible for the densification and sintering processes in the geopolymer paste [99,102]. Therefore, the formation of thermally stable and more compact geopolymers can be concluded due to filling of CMF.

Table 6. Elemental analysis of carbon microfiber/geopolymer composites at elevated temperature

Element	Weight (%)												
	G	5 CG	5 CG 2	5 CG 4	5 CG 8	10 CG	10 CG 2	10 CG 4	10 CG 8	15 CG	15 CG 2	15 CG 4	15 CG 8
Carbon	-	6.98	5.56	9.67	11.54	2.18	2.91	10.15	15.75	11.08	7.58	11.77	9.50
Oxygen	58.02	46.87	38.83	58.39	38.77	54.15	60.01	45.67	53.20	32.27	54.95	56.86	52.60
Sodium	4.06	2.86	1.59	9.91	2.43	1.43	2.82	6.73	9.85	1.59	3.23	16.89	7.35
Magnesium	0.55	1.20	1.35	0.75	1.50	4.29	3.74	1.20	-	1.67	3.83	0.52	0.66
Aluminum	9.24	3.64	3.76	3.61	6.29	4.46	3.81	8.81	2.90	3.47	3.38	3.07	7.77
Silicon	22.58	11.84	13.43	9.81	22.64	17.17	12.81	20.92	16.84	16.56	13.16	8.28	18.14
Sulphur	-	-	-	-	-	0.39	0.18	-	-	0.72	0.31	-	-
Potassium	0.44	0.68	-	-	1.30	0.45	0.20	-	-	0.55	-	-	-
Calcium	5.06	25.89	35.45	7.84	15.49	15.44	13.46	6.49	1.43	32.05	13.52	2.58	3.94

5.6 XRD analysis of geopolymer composites

Figure 27 shows the XRD patterns of samples when exposed to the elevated temperature of 200, 400, and 800 °C. A broad hump at 20–40° 2-theta can be found, which indicated the formation of amorphous gels of geopolymerization [105]. The formation of N-A-S-H gel was found in greater quantity than the C-A-S-H and (C, N)-A-S-H. As the formation of C-A-S-H and (C, N)-A-S-H depend on the availability of calcium ions and pH of the system [104], therefore the extra precipitation of calcium alumina silicate hydrates formation can be attributed to nucleating sites present on BMF. The calcium alumina silicate hydrates were not detected in XRD spectra due to its astable phase. The consistent appearance of broad hump from room temperature to 400 ^{o}C suggested the thermal resistance characteristics of prepared geopolymer composites. The geopolymer composite samples represented their original structural characteristics and there was no any new crystalline phase generated when exposed to elevated temperature upto 400 °C. At room temperature, the several characteristic peaks observed in the XRD pattern were identified as quartz, zeolite, thomsonite, goethite and semicrystalline

hillebrandite. The better durability and thermal stability of geopolymers was ascribed to their zeolite-like structure characteristics [104]. The occurrence of these several characteristic peaks depend on type of aluminosilicate source, type of alkali activator, type of fillers, their mix-design in geopolymer composite, remaining unreacted silica or alumina in geopolymer, remaining unreacted other impurities in geopolymer, etc [102]. Nevertheless, on further increase in elevated temperature to 800 ^{o}C, the diffuse peaks disappeared and new Bragg peaks corresponding to new crystalline phases (i.e. akermanite, nepheline, gehlenite) were detected [106,107]. The mechanism of crystallization at elevated temperature can be explained from the reaction of released calcium, silicon and aluminum from geopolymer gel and unreacted traces of metakaolin/basalt microfibril to form these intermediate products. However, the maximum retention of dimensional stability and strength of geopolymer composites can be expected due to formation of more nepheline phase at increased BMF loading [87].

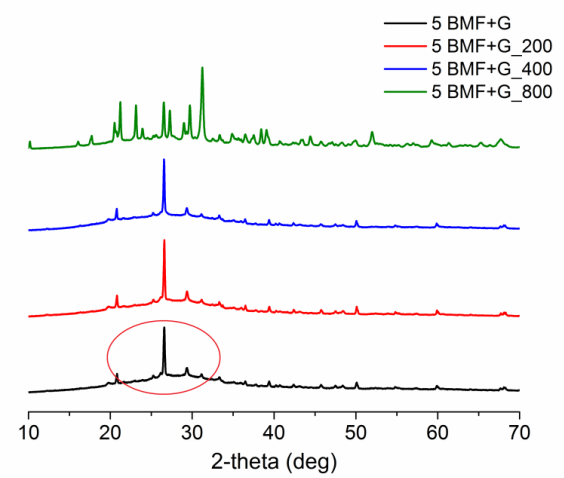

(a) 5 BMF/geopolymer

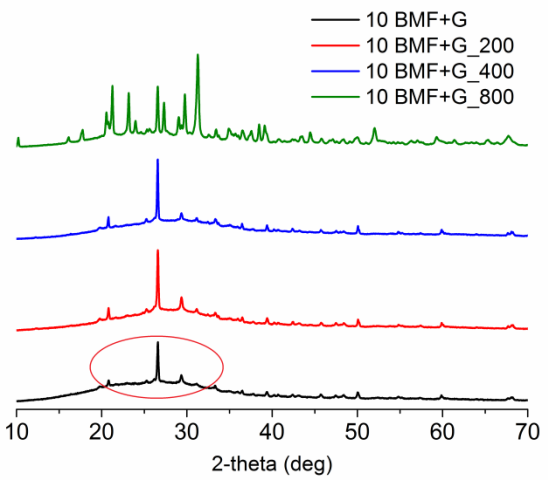

(b) 10 BMF/geopolymer

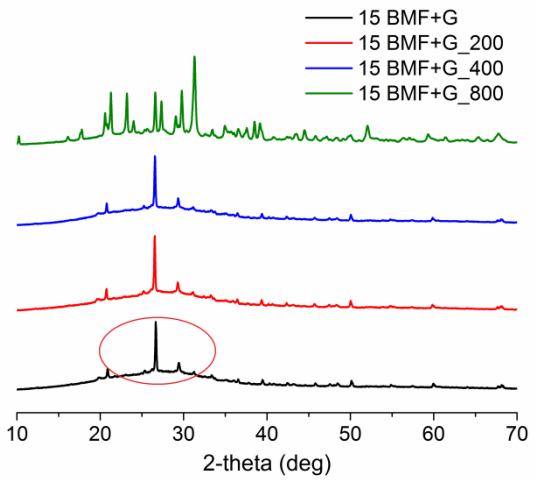

(c) 15 BMF/geopolymer

Figure 27. XRD analysis of basalt microfibril/geopolymer composites at elevated temperature

Similarly, the nature and composition of reaction products in CMF/geopolymer composites were investigated from XRD analysis. Figure 28 shows the XRD patterns of samples when exposed to the elevated temperature of 200, 400, and 800 °C. The formation of amorphous gels of geopolymerization can be confirmed from the broad hump at 20–40° 2-theta [104,105]. The more widening of this peak at higher carbon microfiber loading indicated the increased calcium silicate hydrates and more amorphous gel formation. Furthermore, the consistent

appearance of this diffuse peak from room temperature to 400 ^{o}C suggested the thermal resistance characteristics of prepared geopolymer composites. When exposed to elevated temperature upto 400 °C, the geopolymer composite samples represented their original structural characteristics and there was no any new crystalline phase generated. The several characteristic peaks were identified as quartz, zeolite, thomsonite, goethite and semicrystalline hillebrandite till 400 ^{o}C. As mentioned in previously, the better durability and thermal stability of geopolymers was ascribed to their zeolite-like structure characteristics [104]. Nevertheless, on further increase in elevated temperature to 800 ^{o}C, the diffuse peaks disappeared and new Bragg peaks corresponding to new crystalline phases (i.e. akermanite, nepheline, gehlenite) were detected [106,107]. This indicated the decomposition and crystallization of geopolymers at 800 ^{o}C, which can subsequently deteriorate their mechanical properties.

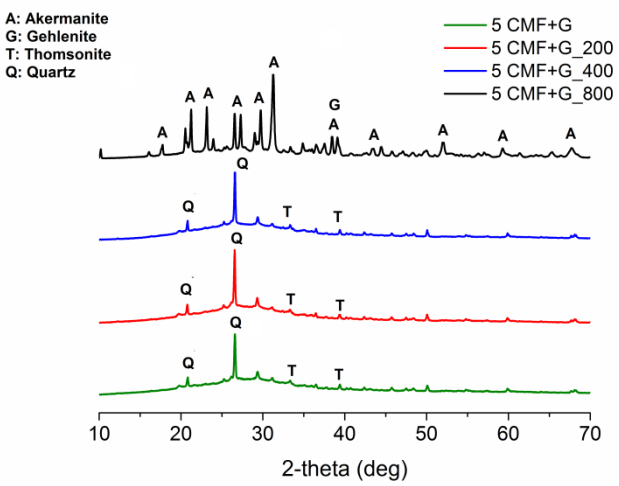

(a). 5 wt % CMF/geopolymer

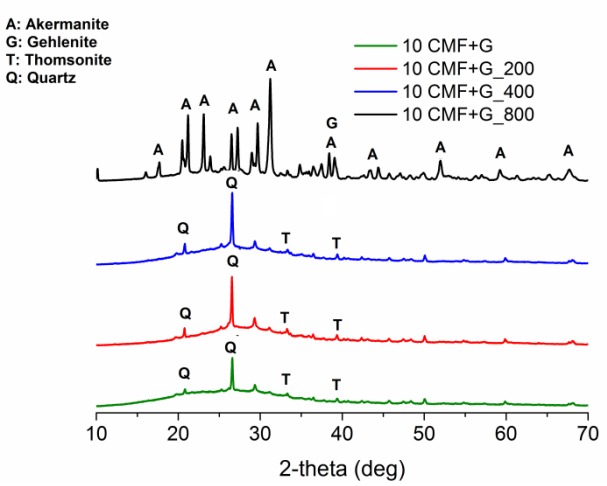

(b). 10 wt % CMF/geopolymer

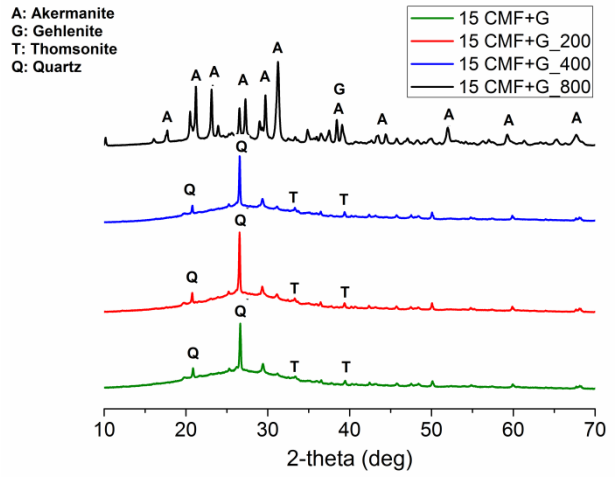

(c). 15 wt % CMF/geopolymer

Figure 28. XRD analysis of carbon microfiber/geopolymer composites

5.7 Physical properties of geopolymer composites

Table 7 illustrates the physical properties (i.e. hardness and bulk density) of the neat geopolymer and BMF/geopolymer composites before and after exposure to elevated temperature. The hardness describes the ability of a material to resist plastic deformation under indentation. Across all range of temperature exposures, the geopolymers showed improved hardness with increased loading of BMF. This explained the uniform distribution of the load on the BMF,

which reduced the penetration of the test ball at the surface of the geopolymer. Further, the higher hardness could be attributed to the extra precipitation of calcium alumina silicate hydrates formation due to nucleating sites present on BMF [27]. However, when the samples were exposed to elevated temperature of 200, 400 and 800 ^{o}C, all the samples showed reduction in bulk density and hardness values. This behavior was attributed to evaporation of water and change in Si/Al ratio (see Table 5) as temperature increased [108,109]. A similar phenomenon was observed previously which resulted in foam like structures by formation and growth of bubbles with increasing the Si/Al ratio [110]. At 800 ^{o}C of elevated temperature exposure, the neat geopolymer showed 13 % reduction in density, whereas 10 wt % basalt microfibril filled geopolymer composites showed 8 % density reduction.

Table 7. Physical properties of basalt microfibril/geopolymer composites at elevated temperature

Temperature (^{o}C)	G		5 BMF+G		10 BMF+G		15 BMF+G	
	Hardness (HV)	Density (kg/m^3)	Hardness (HV)	Density (kg/m^3)	Hardness (HV)	Density (kg/m^3)	Hardness (HV)	Density (kg/m^3)
30	536±46	1510±94	578±58	1560±108	567±60	1570±110	563±64	1550±106
200	395±32	1490±89	402±41	1500±112	419±45	1520±113	483±52	1520±112
400	290±23	1402±86	300±35	1440±109	306±38	1450±115	325±41	1440±113
800	330±37	1310±93	-	-	-	-	-	-

Similarly, the physical properties of neat geopolymer and CMF/geopolymer composites before and after exposure to elevated temperature are illustrated in Table 8. The density was found to reduce with increase in carbon microfiber loading. The carbon microfiber filled geopolymers exhibited significant increase in viscosity due to high aspect ratio and smooth light surfaces of microfibers. This subsequently resulted into the entrapment of more air and thus

possible reduction in density of geopolymer composites than neat geopolymers [43]. From Table 8, the hardness of geopolymer was found to increase with increased loading of CMF across all range of temperature exposures. The similar explanation of uniform distribution of the load on the CMF which reduced the penetration of the test ball at the surface of the geopolymer can be given for enhancement in hardness values. Likewise in the case of BMF, all the CMF/geopolymer composites showed reduction in bulk density and hardness values when exposed to elevated temperature of 200, 400 and 800 ^{o}C. However, drop in hardness of CMF/geopolymer composites was less as compared to BMF/geopolymer composites. This showed intact structure of CMF/geopolymer composites at elevated temperatures due to effective pore-filling effect of carbon micro fibers as compared to BMF.

Table 8. Physical properties of carbon microfiber/geopolymer composites

Temperature (^{o}C)	G		5 CMF+G		10 CMF+G		15 CMF+G	
	Hardness (HV)	Density (kg/m^3)	Hardness (HV)	Density (kg/m^3)	Hardness (HV)	Density (kg/m^3)	Hardness (HV)	Density (kg/m^3)
30	536±46	1510±94	558±52	1480±102	569±51	1490±106	562±55	1480±104
200	395±32	1490±89	489±48	1440±108	494±46	1510±103	482±42	1480±109
400	290±23	1402±86	435±45	1400±111	482±49	1360±113	577±45	1350±112
800	330±37	1310±93	367±41	1270±107	371±45	1260±110	379±43	1220±108

5.8 Compression strength of geopolymer composites

Figure 29 shows the compression strength results of geopolymer and BMF/geopolymer composites before and after exposure to elevated temperatures. The geopolymer composites showed higher compression strength than neat geopolymers over all range of temperature exposures. From stress-strain curve, the neat geopolymer indicated a typical brittle failure mode, whereas geopolymer composites exhibited an extended period of plastic deformation (i.e.

pseudoplastic behavior) unlike short drop at the point of maximum load. This non-linear behavior of geopolymer composites can be explained from the fiber-bridging and sliding after debonding and pulling-out of BMF from the geopolymer matrix. This further indicated more favorable interaction between BMF and the matrix possibly due to a combination of physical and chemical bonding. All samples showed increase in compression strength with increase in temperature till 200 ^{o}C. This behavior was attributed to the formation of discontinuous nano-pores and dehydration shrinkage of geopolymers due to expel of free water at 200 ^{o}C [109]. Nevertheless, with further increase in elevated temperature at 400 and 800 ^{o}C, all samples showed deterioration in compression strength. This phenomenon resulted due to the thermal incompatibility (i.e. differential thermal expansion between geopolymer and BMF), pore pressure effects (i.e. movement of free water and hydroxyls) and possible phase transition in geopolymers [102,108]. At elevated temperature exposure, several events such as evaporation of water adsorbed by N-A-S-H gel, formation of anhydrous products, crystallization of stable anhydrous phases and melting (sintering) occurred, which subsequently deteriorated the mechanical properties [102]. The less deterioration for geopolymer composites indicated the thermal resistance characteristics of geopolymers after the addition of basalt microfibril. This behavior can be further explained from the results of pore area (see Figure 24 (a)), where basalt microfibril acted as effective pore filling agents and exhibited a very limited development of macro-cracks. This decreased the thermal stresses on geopolymer composite pastes at elevated temperature exposure and maintained higher residual mechanical properties [111]. The geopolymer composite of 10 wt % basalt microfibril maintained the residual compressive strengths of 23.13 and 16.08 MPa at 400 ^{o}C and 800 ^{o}C, respectively and thus recording a minimum strength loss of 32 and 43 %, respectively (Table 9). On the other hand, the neat

geopolymers exposed to 800 ^{o}C crumbled into fine particles rather than small broken blocks after the compression strength testing. This indicated the loss of bonding capacity of geopolymers in absence of BMF when exposed to elevated temperatures. Furthermore, the filling of basalt microfibers showed higher compression strength values than the previously reported results on neat OPC when exposed to elevated temperatures [112] (see Figure 30). The significant improvement was found for 800 ^{o}C exposure, where filling of BMF showed higher values of compression strength compared to OPC. The percentage increase over cement was calculated from the Equation (3).

$$\text{Percentage increase over cement} = \frac{\sigma_{gc}-\sigma_{opc}}{\sigma_{opc}} \times 100 \quad (3)$$

Where σ_{gc} is compression strength of geopolymer composites and

σ_{opc} is compression strength of OPC

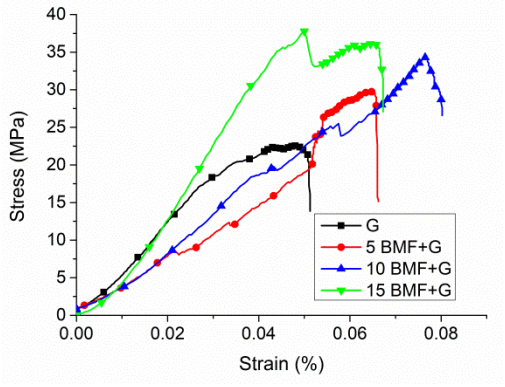

(a) Without exposure

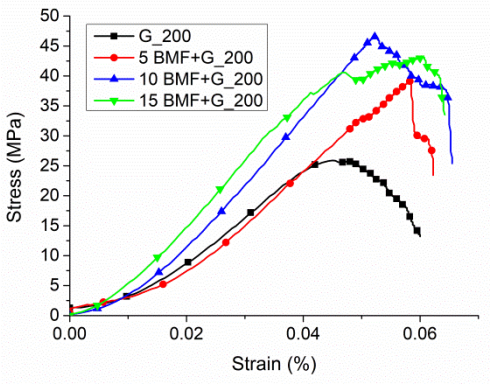

(b) After exposure to 200 ^{o}C

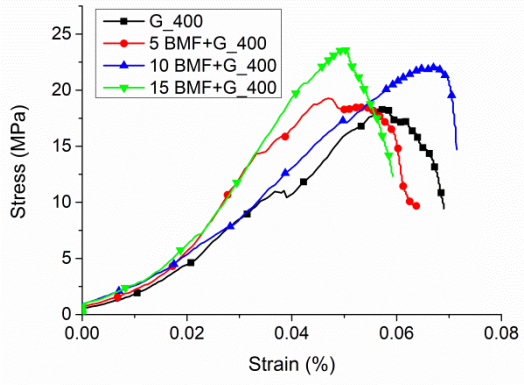

(c) After exposure to 400 ^{o}C

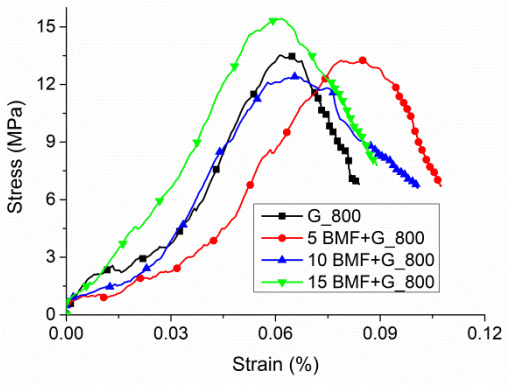

(d) After exposure to 800 ^{o}C

Figure 29. Stress-strain curve for BMF/geopolymer composites

Table 9. Compression strength of basalt microfibril/geopolymer composites at elevated temperature

Temperature (°C)	G	5 BMF+G	10 BMF+G	15 BMF+G	OPC
	Compressive strength (MPa)	Compressive strength (MPa)	Compressive strength (MPa)	Compressive strength (MPa)	Compressive strength (MPa)
30	28.43±2.5	34.82±3.1	34.00±3.2	38.10±3.5	49.5
200	36.61±3.2	39.11±3.5	41.65±3.9	43.85±4.4	48.5
400	14.85±1.9	18.82±2.1	23.13±2.7	21.36±2.5	31.2
800	11.23±2.2	13.74±2.4	16.08±2.5	15.11±2.6	11.3

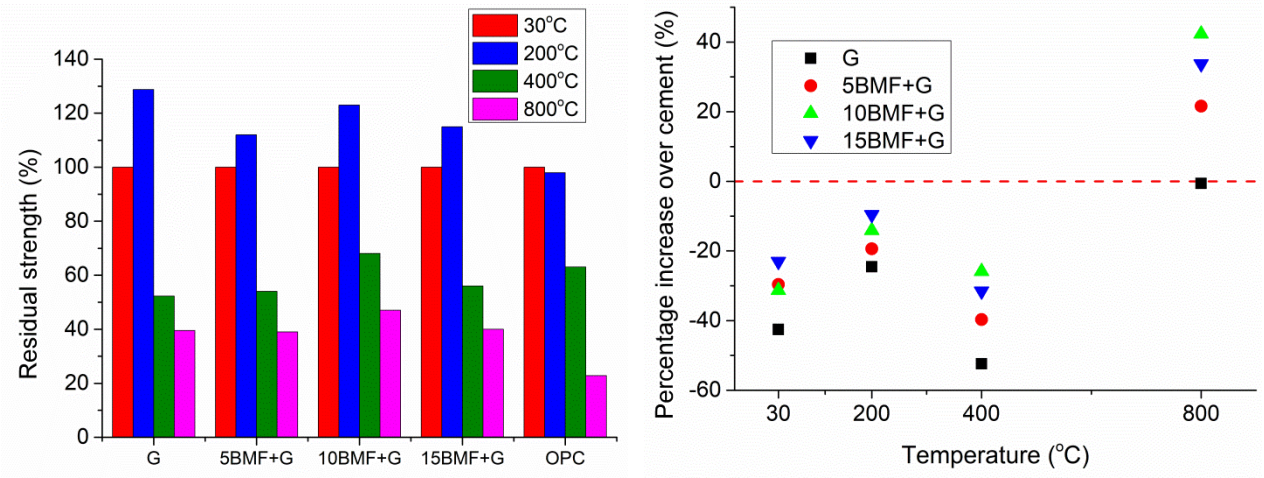

(a) Residual strength (b) Percentage increase

Figure 30. Compression strength comparison of BMF/geopolymer composites with OPC

Similarly, figure 31 showed the compression strength results of geopolymer and CMF/geopolymer composites before and after exposure to elevated temperatures. The stress-strain curve of CMF/geopolymer composites showed larger strain values than BMF/geopolymer

composites. This indicated more pseudoplastic behavior in CMF/geopolymer composites and somewhat brittle behavior of BMF/geopolymer composites. The compression strength of CMF/geopolymer composites was found greater than the compression strength of BMF/geopolymer composites over all range of temperature exposures. The geopolymer composite of 15 wt % carbon micro fiber kept up the residual compressive strengths of 33.55 MPa and 23.96 MPa at 400 ^{o}C and 800 ^{o}C, respectively and therefore recording a minimum strength loss of 19 and 42 %, respectively (Table 10). This proved more favorable interaction of CMF with geopolymer as compared to BMF with geopolymer. Likewise, CMF/geopolymer composites depicted higher compression strength values than the previously reported results of neat OPC when exposed to elevated temperatures (Figure 32). As compared to BMF/geopolymer composites, the percentage increase over OPC strength was found higher in case CMF/geopolymer composites.

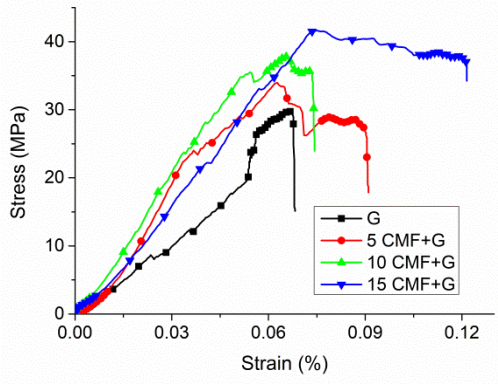

(a) Without exposure

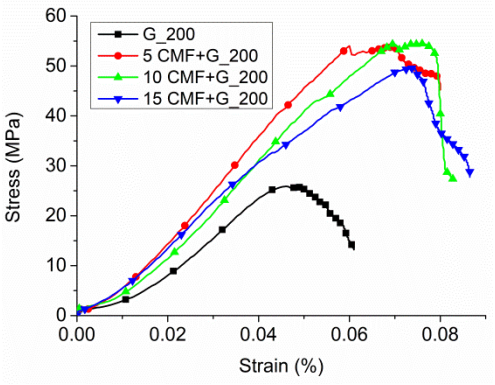

(b) After exposure to 200 ^{o}C

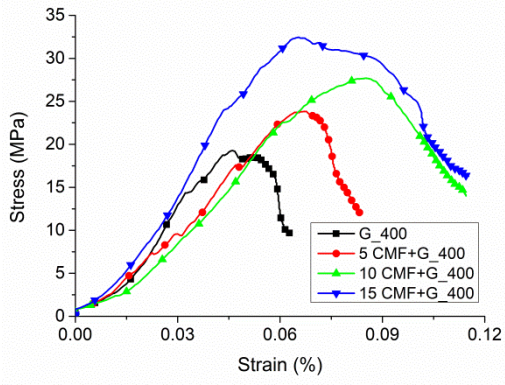

(c) After exposure to 400 ^{o}C

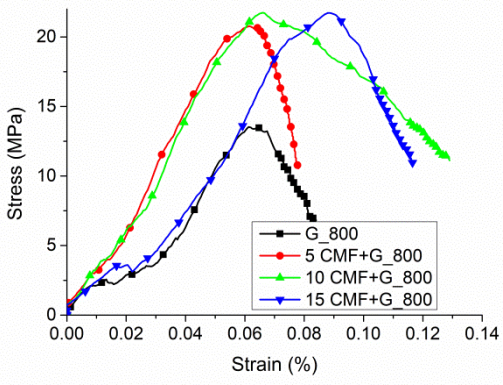

(d) After exposure to 800 ^{o}C

Figure 31. Stress-strain curve for CMF/geopolymer composites

Table 10. Compression strength of carbon microfiber/geopolymer composites

Temperature (°C)	G	5 CMF+G	10 CMF+G	15 CMF+G	OPC
	Compressive strength (MPa)	Compressive strength (MPa)	Compressive strength (MPa)	Compressive strength (MPa)	Compressive strength (MPa)
30	28.43±2.5	38.97±4.1	44.22±4.7	41.33±4.3	49.5
200	36.61±3.2	44.23±4.3	48.77±4.8	45.04±4.6	48.5
400	14.85±2.1	24.21±2.7	30.08±3.3	33.55±3.8	31.2
800	11.23±2.2	19.86±2.3	21.29±2.8	23.96±3.1	11.3

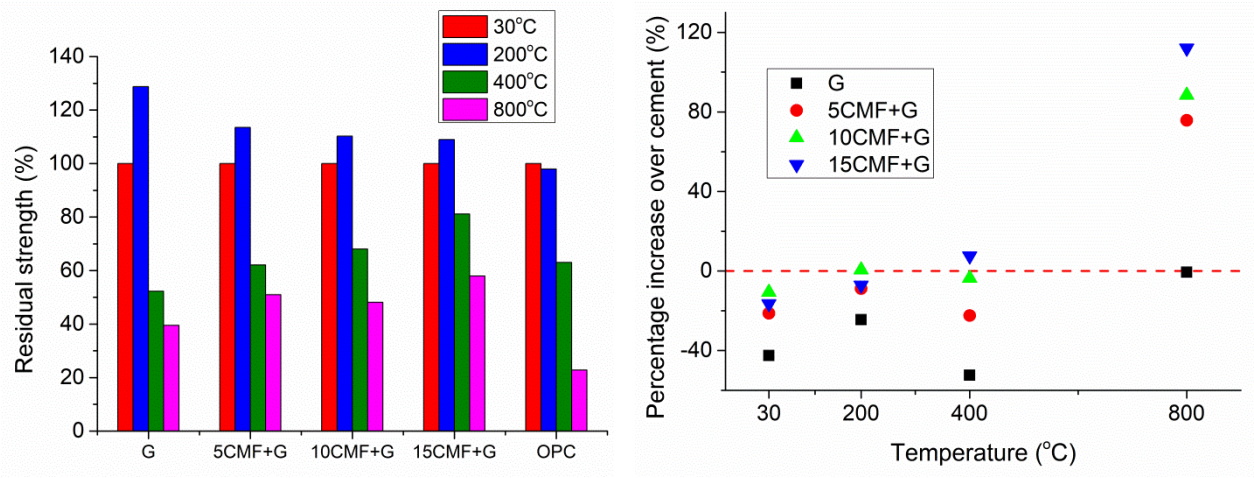

(a) Residual strength (b) Percentage increase

Figure 32. Compression strength comparison of CMF/geopolymer composites with OPC

5.9 Thermo-gravimetric analysis of geopolymer composites

Figure 33 represents the thermo gravimetric analysis curves for the geopolymer composites under different BMF or CMF loading. A sharp decrease in weight before 200 °C was detected for neat geopolymers compared to geopolymer composites because of evaporation of

free water [28]. The weight loss which happened in this temperature range was almost 80 % of the total weight loss. This consequently introduced a very small shrinkage of geopolymers. With additional increase in temperature from 250 °C to 800 °C, a continuous weight loss under slow rate was observed. This indicated the liberation of both surface hydroxyl groups and chemically bonded water by condensation/polymerization, which can subsequently result into the surface-cracking and internal damage of the geopolymer overall structure [113]. Hence, the considerable strength degradation at 800 ^{o}C of temperature exposure can be anticipated as a result of the dehydroxylation attributable to evaporation of surface hydroxyl groups and chemically bonded water [114]. The neat geopolymer showed 87 % of remained mass, while 15 wt % CMF/geopolymer composite showed 90 % of remained mass at 800 ^{o}C. Thus, the higher thermal stability of CMF/geopolymer composite pastes can be elucidated from less release of water by reason of the formation of compact geopolymer systems at higher CMF loading. This can be further justified from results of pore area (see Figure 23 and 24(b)) and zeolite-like characteristics in XRD spectra (see Figure 28).

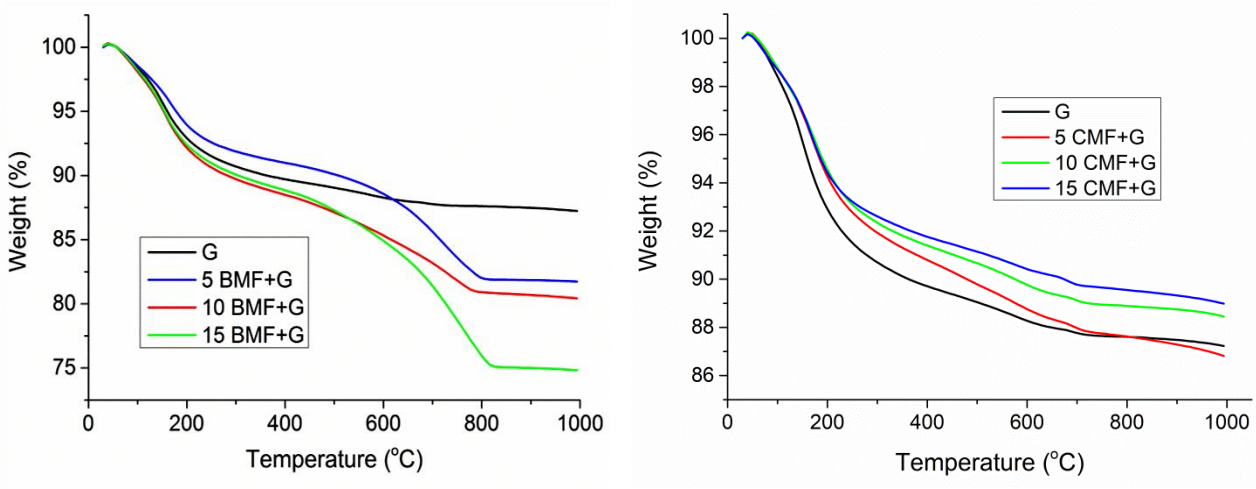

(a) BMF/geopolymer composites (b) CMF/geopolymer composites

Figure 33. (a) Thermal stability of geopolymer composites

6 CHAPTER: CONCLUSIONS

The presented thesis studied the role of basalt and carbon microfibers on improvement in elevated temperature properties of metakaoline based geopolymers. The 30 min dry pulverization of basalt fibrous wastes and carbiso powder was carried out in high energy ball milling to obtain respective basalt and carbon microfibers. Further, the geopolymer composites were prepared by addition of 5, 10 and 15 wt % of carbon/basalt microfibers and later exposed to the elevated temperatures of 200, 400, and 800 °C. The performance of basalt and carbon microfibers was evaluated based on measurements of physical properties, micro structural analysis and compression strength of geopolymer composites. Both geopolymer composites showed higher hardness, higher bulk density and compact structure than neat geopolymers over all range of temperature exposures. This was related to presence of inorganic contents in both microfibers, which produced additional calcium silicate or calcium alumino-silicate and sodium alumino-silicate hydrates. Nevertheless, more compact structure of geopolymers was found after addition of CMF due to effective pore filling characteristics and higher thermal resistance than BMF. On the other hand, the development of wider micro-cracks, higher bright crystals content and the relatively large voids were observed in case of BMF/geopolymer composites. Therefore, the surface-cracking and internal damage of the geopolymer structure was reported to cause the reduction in the strength of geopolymers. The compression strength deteriorated significantly in case of BMF/geopolymer composites than CMF/geopolymer composites at 400 and 800 ^{o}C, which was attributed to thermal incompatibility (i.e. differential thermal expansion between geopolymer and basalt micro fibers), pore pressure effects (i.e. movement of free water and hydroxyls) and possible phase transition in geopolymers at elevated temperature. The less deterioration for CMF/geopolymer composites indicated the thermal resistance characteristics of

geopolymers after the addition of carbon micro fibers, which further decreased the thermal stresses and restricted the swelling of unreacted geopolymer phases. Towards the end, the performance of geopolymer composites was compared with previously reported studies on elevated temperature properties of OPC binders. The geopolymers filled by BMF and CMF showed higher compression strength values than the previously reported results on neat OPC when exposed to 800 ^{o}C. The 5, 10 and 15 wt% BMF filled geopolymers showed 22 %, 42 %, and 34 % increase over OPC respectively, whereas 5, 10 and 15 wt% CMF filled geopolymers showed 76 %, 88 % and 112 % increase over OPC respectively.

7 CHAPTER: FUTURE WORK

In many respects the greatest strength of geopolymer technology is also its greatest weakness in terms of development from a fundamental point of view. The raw materials utilized in geopolymers are incredibly diverse and there is little restriction on the purity, particle size, composition or morphology of material that can be utilized. Therefore, much research has been conducted utilizing a broad range of highly localized and specific raw materials, such as fly ashes from specific power stations, which does not provide general results that may be implemented to all geopolymer systems equally. In spite of various researches on the durability and mechanical properties of fiber reinforced geopolymer composites, a number of challenges still exist and must be considered in order to take advantage of them in infrastructure use. The future research can be devoted to solve the following challenges associated with geopolymer composites

1. The variability of quality and composition of source materials used in geopolymeric cement, (such as fly ash, slag or others) make standardization and comparison between research efforts more complicated.
2. The familiarity and acceptance of geopolymer composite is largely confined to academic and research circles.
3. The chemical process involved in geopolymerization is complex and its understanding is still not mature.
4. Mechanical and durability properties between fibers and geopolymer composites is still limited.
5. The lack of information on the interaction of fibers with geopolymer matrix and toughness of matrix itself.

REFERENCES

[1] G. Fahim Huseien, J. Mirza, M. Ismail, S.K. Ghoshal, A. Abdulameer Hussein, Geopolymer mortars as sustainable repair material: A comprehensive review, Renew. Sustain. Energy Rev. 80 (2017) 54–74. doi:10.1016/j.rser.2017.05.076.

[2] J. Li, S.T. Ng, M. Skitmore, Review of low-carbon refurbishment solutions for residential buildings with particular reference to multi-story buildings in Hong Kong, Renew. Sustain. Energy Rev. 73 (2017) 393–407. doi:10.1016/J.RSER.2017.01.105.

[3] P. Wang, J. Wang, Q. Qin, H. Wang, Life cycle assessment of magnetized fly-ash compound fertilizer production: A case study in China, Renew. Sustain. Energy Rev. 73 (2017) 706–713. doi:10.1016/J.RSER.2017.02.005.

[4] A. de S. Pinto, M.M.C. Bustamante, K. Kisselle, R. Burke, R. Zepp, L.T. Viana, et al., Soil emissions of N_2O, NO, and CO_2 in Brazilian Savannas: Effects of vegetation type, seasonality, and prescribed fires, J. Geophys. Res. 107 (2002) 8089. doi:10.1029/2001JD000342.

[5] P. Chindaprasirt, U. Rattanasak, Improvement of durability of cement pipe with high calcium fly ash geopolymer covering, Constr. Build. Mater. 112 (2016) 956–961. doi:10.1016/j.conbuildmat.2016.03.023.

[6] A. Hassan, M. Arif, M. Shariq, Use of geopolymer concrete for a cleaner and sustainable environment – A review of mechanical properties and microstructure, J. Clean. Prod. 223 (2019) 704–728. doi:10.1016/j.jclepro.2019.03.051.

[7] L. Vickers, A. van Riessen, W. Rickard, Fire-resistant Geopolymers: Role of Fibres and Fillers to Enhance Thermal Properties, 2015.

[8] P. Duxson, A. Fernández-Jiménez, J.L. Provis, G.C. Lukey, A. Palomo, J.S.J. Van

Deventer, Geopolymer technology: The current state of the art, J. Mater. Sci. 42 (2007) 2917–2933. doi:10.1007/s10853-006-0637-z.

[9] J.L. Provis, J.S.J. Van Deventer, Introduction to geopolymers, in: Geopolymers, Elsevier, 2009: pp. 1–11. doi:10.1533/9781845696382.1.

[10] C. Li, H. Sun, L. Li, A review: The comparison between alkali-activated slag (Si + Ca) and metakaolin (Si + Al) cements, Cem. Concr. Res. 40 (2010) 1341–1349. doi:10.1016/j.cemconres.2010.03.020.

[11] N.R. Rakhimova, R.Z. Rakhimov, Reaction products, structure and properties of alkali-activated metakaolin cements incorporated with supplementary materials - A review, J. Mater. Res. Technol. 8 (2019) 1522–1531. doi:10.1016/j.jmrt.2018.07.006.

[12] T.W. Cheng, M.L. Lee, M.S. Ko, T.H. Ueng, S.F. Yang, The heavy metal adsorption characteristics on metakaolin-based geopolymer, Appl. Clay Sci. 56 (2012) 90–96. doi:10.1016/J.CLAY.2011.11.027.

[13] C. Fernández Pereira, Y. Luna, X. Querol, D. Antenucci, J. Vale, Waste stabilization/solidification of an electric arc furnace dust using fly ash-based geopolymers, Fuel. 88 (2009) 1185–1193. doi:10.1016/J.FUEL.2008.01.021.

[14] N. Toniolo, A.R. Boccaccini, Fly ash-based geopolymers containing added silicate waste. A review, Ceram. Int. 43 (2017) 14545–14551. doi:10.1016/J.CERAMINT.2017.07.221.

[15] Z. Ji, Y. Pei, Bibliographic and visualized analysis of geopolymer research and its application in heavy metal immobilization: A review, J. Environ. Manage. 231 (2019) 256–267. doi:10.1016/j.jenvman.2018.10.041.

[16] S. Songpiriyakij, T. Pulngern, P. Pungpremtrakul, C. Jaturapitakkul, Anchorage of steel bars in concrete by geopolymer paste, Mater. Des. 32 (2011) 3021–3028.

doi:10.1016/J.MATDES.2011.01.048.

[17] R.A.A. Boca Santa, C. Soares, H.G. Riella, Geopolymers with a high percentage of bottom ash for solidification/immobilization of different toxic metals, J. Hazard. Mater. 318 (2016) 145–153. doi:10.1016/J.JHAZMAT.2016.06.059.

[18] B.I. El-Eswed, O.M. Aldagag, F.I. Khalili, Efficiency and mechanism of stabilization/solidification of Pb(II), Cd(II), Cu(II), Th(IV) and U(VI) in metakaolin based geopolymers, Appl. Clay Sci. 140 (2017) 148–156. doi:10.1016/J.CLAY.2017.02.003.

[19] J. Davidovits, Ph. Davidovits, Geopolymer Chemistry and Applications, 2008.

[20] Z. Xu, Z. Yang, J. Zhang, M. Zhang, Preparation technology and properties of sludge-high calcium coal waste geopolymer, Fuhe Cailiao Xuebao/Acta Mater. Compos. Sin. 30 (2013) 113–118.

[21] Z. Zhang, J.L. Provis, A. Reid, H. Wang, Geopolymer foam concrete: An emerging material for sustainable construction, Constr. Build. Mater. 56 (2014) 113–127. doi:10.1016/j.conbuildmat.2014.01.081.

[22] F.U.A. Shaikh, A. Hosan, Mechanical properties of steel fibre reinforced geopolymer concretes at elevated temperatures, Constr. Build. Mater. 114 (2016) 15–28. doi:10.1016/j.conbuildmat.2016.03.158.

[23] P.K. Sarker, S. Kelly, Z. Yao, Effect of fire exposure on cracking, spalling and residual strength of fly ash geopolymer concrete, Mater. Des. 63 (2014) 584–592. doi:10.1016/j.matdes.2014.06.059.

[24] S.M. Abbasi, H. Ahmadi, G. Khalaj, B. Ghasemi, Microstructure and mechanical properties of a metakaolinite-based geopolymer nanocomposite reinforced with carbon nanotubes, Ceram. Int. 42 (2016) 15171–15176. doi:10.1016/j.ceramint.2016.06.080.

[25] O.A. Abdulkareem, A.M. Mustafa Al Bakri, H. Kamarudin, I. Khairul Nizar, A.A. Saif, Effects of elevated temperatures on the thermal behavior and mechanical performance of fly ash geopolymer paste, mortar and lightweight concrete, Constr. Build. Mater. 50 (2014) 377–387. doi:10.1016/j.conbuildmat.2013.09.047.

[26] L.P. Zawada, R.C. Wetherhold, The effects of thermal fatigue on a SiC fibre/aluminosilicate glass composite, J. Mater. Sci. 26 (1991) 648–654. doi:10.1007/BF00588299.

[27] B. Singh, G. Ishwarya, M. Gupta, S.K. Bhattacharyya, Geopolymer concrete: A review of some recent developments, Constr. Build. Mater. 85 (2015) 78–90. doi:10.1016/j.conbuildmat.2015.03.036.

[28] D.L.Y. Kong, J.G. Sanjayan, K. Sagoe-Crentsil, Comparative performance of geopolymers made with metakaolin and fly ash after exposure to elevated temperatures, Cem. Concr. Res. 37 (2007) 1583–1589. doi:10.1016/j.cemconres.2007.08.021.

[29] N. Kabay, Abrasion resistance and fracture energy of concretes with basalt fiber, Constr. Build. Mater. 50 (2014) 95–101. doi:10.1016/j.conbuildmat.2013.09.040.

[30] V.A. Rybin, A. V. Utkin, N.I. Baklanova, Alkali resistance, microstructural and mechanical performance of zirconia-coated basalt fibers, Cem. Concr. Res. 53 (2013) 1–8. doi:10.1016/j.cemconres.2013.06.002.

[31] V. Dhand, G. Mittal, K.Y. Rhee, S.J. Park, D. Hui, A short review on basalt fiber reinforced polymer composites, Compos. Part B Eng. 73 (2015) 166–180. doi:10.1016/j.compositesb.2014.12.011.

[32] V. Fiore, T. Scalici, G. Di Bella, A. Valenza, A review on basalt fibre and its composites, Compos. Part B Eng. 74 (2015) 74–94. doi:10.1016/j.compositesb.2014.12.034.

[33] M. Saafi, L. Tang, J. Fung, M. Rahman, J. Liggat, Enhanced properties of graphene/fly ash geopolymeric composite cement, Cem. Concr. Res. 67 (2015) 292–299. doi:10.1016/j.cemconres.2014.08.011.

[34] S. Yan, P. He, D. Jia, Z. Yang, X. Duan, S. Wang, et al., Effect of fiber content on the microstructure and mechanical properties of carbon fiber felt reinforced geopolymer composites, Ceram. Int. 42 (2016) 7837–7843. doi:10.1016/j.ceramint.2016.01.197.

[35] S. Parveen, S. Rana, R. Fangueiro, M.C. Paiva, Microstructure and mechanical properties of carbon nanotube reinforced cementitious composites developed using a novel dispersion technique, Cem. Concr. Res. 73 (2015) 215–227. doi:10.1016/j.cemconres.2015.03.006.

[36] S. Ahmad, R.A. Khushnood, P. Jagdale, J.M. Tulliani, G.A. Ferro, High performance self-consolidating cementitious composites by using micro carbonized bamboo particles, Mater. Des. 76 (2015) 223–229. doi:10.1016/j.matdes.2015.03.048.

[37] F. Pacheco-Torgal, J. Castro-Gomes, S. Jalali, Alkali-activated binders: A review. Part 1. Historical background, terminology, reaction mechanisms and hydration products, Constr. Build. Mater. 22 (2008) 1305–1314. doi:10.1016/j.conbuildmat.2007.10.015.

[38] N. Asim, M. Alghoul, M. Mohammad, M.H. Amin, M. Akhtaruzzaman, N. Amin, et al., Emerging sustainable solutions for depollution: Geopolymers, Constr. Build. Mater. 199 (2019) 540–548. doi:10.1016/j.conbuildmat.2018.12.043.

[39] J. Davidovits, Geopolymers: Ceramic-like inorganic polymers, J. Ceram. Sci. Technol. 8 (2017) 335–350. doi:10.4416/JCST2017-00038.

[40] J.L. Provis, J.S.J. van Deventer, Geopolymers, Woodhead Publishing Limited, 2009. doi:10.1533/9781845696382.

[41] C. Ng, U.J. Alengaram, L.S. Wong, K.H. Mo, M.Z. Jumaat, S. Ramesh, A review on microstructural study and compressive strength of geopolymer mortar, paste and concrete, Constr. Build. Mater. 186 (2018) 550–576. doi:10.1016/j.conbuildmat.2018.07.075.

[42] F. Pacheco-Torgal, J. Castro-Gomes, S. Jalali, Alkali-activated binders: A review, Constr. Build. Mater. 22 (2008) 1305–1314. doi:10.1016/j.conbuildmat.2007.10.015.

[43] G. Masi, W.D.A. Rickard, M.C. Bignozzi, A. Van Riessen, The effect of organic and inorganic fibres on the mechanical and thermal properties of aluminate activated geopolymers, Compos. Part B Eng. 76 (2015) 218–228. doi:10.1016/j.compositesb.2015.02.023.

[44] S.A. Rasaki, Z. Bingxue, R. Guarecuco, T. Thomas, Y. Minghui, Geopolymer for use in heavy metals adsorption, and advanced oxidative processes: A critical review, J. Clean. Prod. 213 (2019) 42–58. doi:10.1016/j.jclepro.2018.12.145.

[45] Joseph Davidovits, Geopolymers: Inorganic polymeric new materials, J. Therm. Anal. 37 (1991) 1633–1656.

[46] J. Davidovits, Properities of Geopolymer Cements, in: First Int. Conf. Alkaline Cem. Concr., 1994: pp. 131–149.

[47] J.G.S. van Jaarsveld, J.S.J. van Deventer, G.C. Lukey, The characterisation of source materials in fly ash-based geopolymers, Mater. Lett. 57 (2003) 1272–1280. doi:10.1016/S0167-577X(02)00971-0.

[48] J.L. Provis, G.C. Lukey, J.S.J. van Deventer, Do Geopolymers Actually Contain Nanocrystalline Zeolites? A Reexamination of Existing Results, Chem. Mater. 17 (2005) 3075–3085. doi:10.1021/cm050230i.

[49] K. Komnitsas, D. Zaharaki, Geopolymerisation: A review and prospects for the minerals

industry, Miner. Eng. 20 (2007) 1261–1277. doi:10.1016/j.mineng.2007.07.011.

[50] H. Wang, H. Li, F. Yan, Synthesis and mechanical properties of metakaolinite-based geopolymer, Colloids Surfaces A Physicochem. Eng. Asp. 268 (2005) 1–6. doi:10.1016/j.colsurfa.2005.01.016.

[51] P. Duxson, J.L. Provis, G.C. Lukey, S.W. Mallicoat, W.M. Kriven, J.S.J. van Deventer, Understanding the relationship between geopolymer composition, microstructure and mechanical properties, Colloids Surfaces A Physicochem. Eng. Asp. 269 (2005) 47–58. doi:10.1016/j.colsurfa.2005.06.060.

[52] F. Messina, C. Ferone, F. Colangelo, R. Cioffi, Low temperature alkaline activation of weathered fly ash: Influence of mineral admixtures on early age performance, Constr. Build. Mater. 86 (2015) 169–177. doi:10.1016/j.conbuildmat.2015.02.069.

[53] K.M. Liew, A.O. Sojobi, L.W. Zhang, Green concrete: Prospects and challenges, Constr. Build. Mater. 156 (2017) 1063–1095. doi:10.1016/j.conbuildmat.2017.09.008.

[54] A.R. Sakulich, Reinforced geopolymer composites for enhanced material greenness and durability, Sustain. Cities Soc. 1 (2011) 195–210. doi:10.1016/j.scs.2011.07.009.

[55] F.U.A. Shaikh, Review of mechanical properties of short fibre reinforced geopolymer composites, Constr. Build. Mater. 43 (2013) 37–49. doi:10.1016/j.conbuildmat.2013.01.026.

[56] J.W.Phair, J.S.J. van Deventer, Effect of silicate activator pH on the leaching and material characteristics of effect of waste-based inorganic polymers, Miner. Eng. 14 (2001) 289–304.

[57] J.G.S. van Jaarsveld, J.S.J. van Deventer, Effect of the Alkali Metal Activator on the Properties of Fly Ash-Based Geopolymers, Ind. Eng. Chem. Res. 38 (1999) 3932–3941.

doi:10.1021/ie980804b.

[58] A.S. de Vargas, D.C.C. Dal Molin, A.C.F. Vilela, F.J. da Silva, B. Pavão, H. Veit, The effects of Na2O/SiO2molar ratio, curing temperature and age on compressive strength, morphology and microstructure of alkali-activated fly ash-based geopolymers, Cem. Concr. Compos. 33 (2011) 653–660. doi:10.1016/j.cemconcomp.2011.03.006.

[59] H. Xu, J.S.J. Van Deventer, Geopolymerisation of multiple minerals, Miner. Eng. 15 (2002) 1131–1139. doi:10.1016/S0892-6875(02)00255-8.

[60] J.G.. van Jaarsveld, J.S.. van Deventer, G.. Lukey, The effect of composition and temperature on the properties of fly ash- and kaolinite-based geopolymers, Chem. Eng. J. 89 (2002) 63–73. doi:10.1016/S1385-8947(02)00025-6.

[61] C.Y. Heah, H. Kamarudin, A.M.M. Al Bakri, M. Binhussain, M. Luqman, I.K. Nizar, et al., Effect of Curing Profile on Kaolin-based Geopolymers, Phys. Procedia. 22 (2011) 305–311. doi:10.1016/j.phpro.2011.11.048.

[62] P. Rovnaník, Effect of curing temperature on the development of hard structure of metakaolin-based geopolymer, Constr. Build. Mater. 24 (2010) 1176–1183. doi:10.1016/j.conbuildmat.2009.12.023.

[63] C.K. Yip, G.C. Lukey, J.S.J. Van Deventer, The coexistence of geopolymeric gel and calcium silicate hydrate at the early stage of alkaline activation, Cem. Concr. Res. 35 (2005) 1688–1697. doi:10.1016/j.cemconres.2004.10.042.

[64] C.K. Yip, G.C. Lukey, J.L. Provis, J.S.J. van Deventer, Effect of calcium silicate sources on geopolymerisation, Cem. Concr. Res. 38 (2008) 554–564. doi:10.1016/j.cemconres.2007.11.001.

[65] S. Puligilla, P. Mondal, Role of slag in microstructural development and hardening of fly

ash-slag geopolymer, Cem. Concr. Res. 43 (2013) 70–80. doi:10.1016/j.cemconres.2012.10.004.

[66] A. Kusbiantoro, M.S. Ibrahim, K. Muthusamy, A. Alias, Development of Sucrose and Citric Acid as the Natural based Admixture for Fly Ash based Geopolymer, Procedia Environ. Sci. 17 (2013) 596–602. doi:10.1016/j.proenv.2013.02.075.

[67] J.G. Jang, N.K. Lee, H.K. Lee, Fresh and hardened properties of alkali-activated fly ash/slag pastes with superplasticizers, Constr. Build. Mater. 50 (2014) 169–176. doi:10.1016/j.conbuildmat.2013.09.048.

[68] S. Bernal, R. De Gutierrez, S. Delvasto, E. Rodriguez, Performance of an alkali-activated slag concrete reinforced with steel fibers, Constr. Build. Mater. 24 (2010) 208–214. doi:10.1016/j.conbuildmat.2007.10.027.

[69] Q. Zhao, B. Nair, T. Rahimian, P. Balaguru, Novel geopolymer based composites with enhanced ductility, J. Mater. Sci. 42 (2007) 3131–3137. doi:10.1007/s10853-006-0527-4.

[70] D.P. Dias, C. Thaumaturgo, Fracture toughness of geopolymeric concretes reinforced with basalt fibers, Cem. Concr. Compos. 27 (2005) 49–54. doi:10.1016/j.cemconcomp.2004.02.044.

[71] W. Li, J. Xu, Mechanical properties of basalt fiber reinforced geopolymeric concrete under impact loading, Mater. Sci. Eng. A. 505 (2009) 178–186. doi:10.1016/j.msea.2008.11.063.

[72] R.E. Lyon, P.N. Balaguru, A. Foden, U. Sorathia, J. Davidovits, M. Davidovics, Fire-resistant aluminosilicate composites, Fire Mater. 21 (1997) 67–73. doi:10.1002/(SICI)1099-1018(199703)21:2<67::AID-FAM596>3.0.CO;2-N.

[73] R.E. Lyon, U. Sorathia, P.N. Balaguru, A. Foden, J. Davidovits, M. Davidovics, Fire

Response of Geopolymer Structural Composites, Proc. First Int. Conf. Fiber Compos. Infrastruct. (ICCI ’96). (1996).

[74] H. Zhang, V. Kodur, L. Cao, S. Qi, Fiber Reinforced Geopolymers for Fire Resistance Applications, Procedia Eng. 71 (2014) 153–158. doi:10.1016/j.proeng.2014.04.022.

[75] T. Alomayri, F.U.A. Shaikh, I.M. Low, Mechanical and thermal properties of ambient cured cotton fabric-reinforced fly ash-based geopolymer composites, Ceram. Int. 40 (2014) 14019–14028. doi:10.1016/j.ceramint.2014.05.128.

[76] P. He, D. Jia, T. Lin, M. Wang, Y. Zhou, Effects of high-temperature heat treatment on the mechanical properties of unidirectional carbon fiber reinforced geopolymer composites, Ceram. Int. 36 (2010) 1447–1453. doi:10.1016/j.ceramint.2010.02.012.

[77] W.M. Kriven, J. Bell, M. Gordon, Geopolymer Refractories for the Glass Manufacturing Industry, in: Wiley Online Libr., 2008: pp. 57–80. doi:10.1002/9780470294857.ch5.

[78] D. Pernica, P.N.B. Reis, J.A.M. Ferreira, P. Louda, Effect of test conditions on the bending strength of a geopolymer- reinforced composite, J. Mater. Sci. 45 (2010) 744–749. doi:10.1007/s10853-009-3994-6.

[79] L. Zuda, P. Bayer, P. Rovnaník, R. Černý, Mechanical and hydric properties of alkali-activated aluminosilicate composite with electrical porcelain aggregates, Cem. Concr. Compos. 30 (2008) 266–273. doi:10.1016/j.cemconcomp.2007.11.003.

[80] C.G. Papakonstantinou, J.W. Giancaspro, P.N. Balaguru, Fire response and mechanical behavior of polysialate syntactic foams, Compos. Part A Appl. Sci. Manuf. 39 (2008) 75–84. doi:10.1016/j.compositesa.2007.08.029.

[81] L. Zuda, R. Černý, Measurement of linear thermal expansion coefficient of alkali-activated aluminosilicate composites up to 1000 °C, Cem. Concr. Compos. 31 (2009)

263–267. doi:10.1016/j.cemconcomp.2009.02.002.

[82] H. Wang, H. Li, F. Yan, Synthesis and tribological behavior of metakaolinite-based geopolymer composites, Mater. Lett. 59 (2005) 3976–3981. doi:10.1016/j.matlet.2004.08.049.

[83] E. Kamseu, A. Rizzuti, C. Leonelli, D. Perera, Enhanced thermal stability in K2O-metakaolin-based geopolymer concretes by Al2O3 and SiO2 fillers addition, J. Mater. Sci. 45 (2010) 1715–1724. doi:10.1007/s10853-009-4108-1.

[84] K. Hemra, P. Aungkavattana, Effect of cordierite addition on compressive strength and thermal stability of metakaolin based geopolymer, Adv. Powder Technol. 27 (2016) 1021–1026. doi:10.1016/j.apt.2016.04.019.

[85] T.S. Lin, D.C. Jia, P.G. He, M.R. Wang, Thermal-mechanical properties of short carbon fiber reinforced geopolymer matrix composites subjected to thermal load, J. Cent. South Univ. Technol. (English Ed. 16 (2009) 881–886. doi:10.1007/s11771-009-0146-8.

[86] S.A. Bernal, J. Bejarano, C. Garzón, R. Mejía De Gutiérrez, S. Delvasto, E.D. Rodríguez, Performance of refractory aluminosilicate particle/fiber-reinforced geopolymer composites, Compos. Part B Eng. 43 (2012) 1919–1928. doi:10.1016/j.compositesb.2012.02.027.

[87] A.M. Rashad, A.A. Hassan, S.R. Zeedan, An investigation on alkali-activated Egyptian metakaolin pastes blended with quartz powder subjected to elevated temperatures, Appl. Clay Sci. 132–133 (2016) 366–376. doi:10.1016/j.clay.2016.07.002.

[88] H.Y. Zhang, V. Kodur, S.L. Qi, L. Cao, B. Wu, Development of metakaolin–fly ash based geopolymers for fire resistance applications, Constr. Build. Mater. 55 (2014) 38–45. doi:10.1016/j.conbuildmat.2014.01.040.

[89] A.C.C. Trindade, F. de A. Silva, H.A. Alcamand, P.H.R. Borges, On The Mechanical Behavior of Metakaolin Based Geopolymers Under Elevated Temperatures, Mater. Res. 20 (2017) 265–272. doi:10.1590/1980-5373-mr-2017-0101.

[90] Y.-M. Liew, C.-Y. Heah, A.B. Mohd Mustafa, H. Kamarudin, Structure and properties of clay-based geopolymer cements: A review, Prog. Mater. Sci. 83 (2016) 595–629. doi:10.1016/j.pmatsci.2016.08.002.

[91] C.Y. Heah, H. Kamarudin, A.M. Mustafa Al Bakri, M. Bnhussain, M. Luqman, I. Khairul Nizar, et al., Study on solids-to-liquid and alkaline activator ratios on kaolin-based geopolymers, Constr. Build. Mater. 35 (2012) 912–922. doi:10.1016/j.conbuildmat.2012.04.102.

[92] G. Varga, The structure of kaolinite and metakaolinite, Epa. - J. Silic. Based Compos. Mater. 59 (2007) 6–9. doi:10.14382/epitoanyag-jsbcm.2007.2.

[93] P.S. Singh, T. Bastow, M. Trigg, Structural studies of geopolymers by 29Si and 27Al MAS-NMR, J. Mater. Sci. 40 (2005) 3951–3961. doi:10.1007/s10853-005-1915-x.

[94] V. Baheti, S. Naeem, J. Militky, M. Okrasa, B. Tomkova, Optimized preparation of activated carbon nanoparticles from acrylic fibrous wastes, Fibers Polym. 16 (2015) 2193–2201. doi:10.1007/s12221-015-5364-0.

[95] V. Baheti, J. Militky, R. Mishra, B.K. Behera, Thermomechanical properties of glass fabric/epoxy composites filled with fly ash, Compos. Part B Eng. 85 (2016) 268–276. doi:10.1016/J.COMPOSITESB.2015.09.049.

[96] T. Hemalatha, M. Gunavadhi, B. Bhuvaneshwari, S. Sasmal, N.R. Iyer, Characterization of micro- and nano- modified cementitious system using micro analytical techniques, Cem. Concr. Compos. 58 (2015) 114–128. doi:10.1016/j.cemconcomp.2015.01.004.

[97] ASTM-C948, Standard Test Method for Dry and Wet Bulk Density , Water Absorption , and Apparent Porosity of Thin Sections of Glass-Fiber Reinforced, Am. Soc. Test. Mater. West Conshohocken, PA, USA. 81 (2014) 24–25. doi:10.1520/C0948-81R09.1.

[98] D. Asprone, E. Cadoni, F. Iucolano, A. Prota, Analysis of the strain-rate behavior of a basalt fiber reinforced natural hydraulic mortar, Cem. Concr. Compos. 53 (2014) 52–58. doi:10.1016/j.cemconcomp.2014.06.009.

[99] P.S. Deb, P.K. Sarker, S. Barbhuiya, Effects of nano-silica on the strength development of geopolymer cured at room temperature, Constr. Build. Mater. 101 (2015) 675–683. doi:10.1016/j.conbuildmat.2015.10.044.

[100] P.S. Deb, P.K. Sarker, S. Barbhuiya, Sorptivity and acid resistance of ambient-cured geopolymer mortars containing nano-silica, Cem. Concr. Compos. 72 (2016) 235–245. doi:10.1016/j.cemconcomp.2016.06.017.

[101] C. Jiang, K. Fan, F. Wu, D. Chen, Experimental study on the mechanical properties and microstructure of chopped basalt fibre reinforced concrete, Mater. Des. 58 (2014) 187–193. doi:10.1016/j.matdes.2014.01.056.

[102] J. Ye, W. Zhang, D. Shi, Effect of elevated temperature on the properties of geopolymer synthesized from calcined ore-dressing tailing of bauxite and ground-granulated blast furnace slag, Constr. Build. Mater. 69 (2014) 41–48. doi:10.1016/j.conbuildmat.2014.07.002.

[103] H.Y. Zhang, V. Kodur, S.L. Qi, B. Wu, Characterizing the bond strength of geopolymers at ambient and elevated temperatures, Cem. Concr. Compos. 58 (2015) 40–49. doi:10.1016/j.cemconcomp.2015.01.006.

[104] Y.J. Zhang, S. Li, Y.C. Wang, D.L. Xu, Microstructural and strength evolutions of

geopolymer composite reinforced by resin exposed to elevated temperature, J. Non. Cryst. Solids. 358 (2012) 620–624. doi:10.1016/j.jnoncrysol.2011.11.006.

[105] X. Guo, H. Shi, W.A. Dick, Compressive strength and microstructural characteristics of class C fly ash geopolymer, Cem. Concr. Compos. 32 (2010) 142–147. doi:10.1016/j.cemconcomp.2009.11.003.

[106] P. Sturm, G.J.G. Gluth, S. Simon, H.J.H. Brouwers, H.C. Kühne, The effect of heat treatment on the mechanical and structural properties of one-part geopolymer-zeolite composites, Thermochim. Acta. 635 (2016) 41–58. doi:10.1016/j.tca.2016.04.015.

[107] M.Z.N. Khan, F. uddin A. Shaikh, Y. Hao, H. Hao, Synthesis of high strength ambient cured geopolymer composite by using low calcium fly ash, Constr. Build. Mater. 125 (2016) 809–820. doi:10.1016/j.conbuildmat.2016.08.097.

[108] S.A. Omer, R. Demirboga, W.H. Khushefati, Relationship between compressive strength and UPV of GGBFS based geopolymer mortars exposed to elevated temperatures, Constr. Build. Mater. 94 (2015) 189–195. doi:10.1016/j.conbuildmat.2015.07.006.

[109] N. Ranjbar, M. Mehrali, U.J. Alengaram, H.S.C. Metselaar, M.Z. Jumaat, Compressive strength and microstructural analysis of fly ash/palm oil fuel ash based geopolymer mortar under elevated temperatures, Constr. Build. Mater. 65 (2014) 114–121. doi:10.1016/j.conbuildmat.2014.04.064.

[110] P. Rovnaník, P. Bayer, P. Rovnaníková, Characterization of alkali activated slag paste after exposure to high temperatures, Constr. Build. Mater. 47 (2013) 1479–1487. doi:10.1016/j.conbuildmat.2013.06.070.

[111] G. Roviello, L. Ricciotti, C. Ferone, F. Colangelo, O. Tarallo, Fire resistant melamine based organic-geopolymer hybrid composites, Cem. Concr. Compos. 59 (2015) 89–99.

doi:10.1016/j.cemconcomp.2015.03.007.

[112] M. Liu, Y. Zhao, Y. Xiao, Z. Yu, Performance of cement pastes containing sewage sludge ash at elevated temperatures, Constr. Build. Mater. 211 (2019) 785–795. doi:10.1016/j.conbuildmat.2019.03.290.

[113] Z. Pan, J.G. Sanjayan, F. Collins, Effect of transient creep on compressive strength of geopolymer concrete for elevated temperature exposure, Cem. Concr. Res. 56 (2014) 182–189. doi:10.1016/j.cemconres.2013.11.014.

[114] H.Y. Zhang, V. Kodur, B. Wu, L. Cao, F. Wang, Thermal behavior and mechanical properties of geopolymer mortar after exposure to elevated temperatures, Constr. Build. Mater. 109 (2016) 17–24. doi:10.1016/j.conbuildmat.2016.01.043.

LIST OF PUBLICATIONS

Publications in International Journals:

1. P. Behera, V. Baheti, J. Militky, and S. Naeem, "Microstructure and mechanical properties of carbon microfiber reinforced geopolymers at elevated temperatures," *Constr. Build. Mater.*, vol. 160, pp. 733–743, Jan. 2018.
2. P. Behera, V. Baheti, J. Militky, and P. Louda, "Elevated temperature properties of basalt microfibril filled geopolymer composites," *Constr. Build. Mater.*, vol. 163, pp. 850–860, Feb. 2018.
3. M. Salman Naeem *et al.*, "Impact of carbonization temperature on activated carbon web for EMI shielding and ohmic heating," *Vlakna a Text.*, vol. 25, no. 3, pp. 57–62, 2018.
4. M. Salman Naeem *et al.*, "Impact of carbonization temperature on activated carbon web for EMI shielding and ohmic heating," *Vlakna a Text.*, vol. 25, no. 3, pp. 57–62, 2018.
5. S. Faheem, V. Baheti, P. Behera, and S. Naeem, "Development of flame retardant high loft polyester nonwovens," *J. Text. Inst.*, vol. 108, no. 8, pp. 1357–1364, Aug. 2017.
6. S. Naeem, V. Baheti, J. Militky, J. Wiener, P. Behera, and A. Ashraf, "Sorption properties of iron impregnated activated carbon web for removal of methylene blue from aqueous media," *Fibers Polym.*, vol. 17, no. 8, pp. 1245–1255, Aug. 2016.

International Conference Papers and Book chapters

1. P. Behera, V. Baheti, A. Koch, J. Wiener, J. Militky, and T. Ltd, Feasibility analysis - using recycled carbon short fibres for trc, 9th International Conference on Nanomaterials - Research & Application, 2018.
2. P. Behera, V. Baheti, J. Militky, P. Louda, mechanical performance of basalt microfibril filled geopolymer composites at elevated temperature, the 25th annual international conference on composites/nano engineering (icce-25), 2017.

3. P. Behera, V. Baheti, J. Militky, P. Louda, microstructure and mechanical properties of carbon microfiber reinforced geopolymers at elevated temperatures, the 25th annual international conference on composites/nano engineering (icce-25), 2017.
4. S. Naeem, S. Javed, V. Baheti, J. Militky, Z. Ahmed, P. Behera, Effect of temperature, heating rate and holding time on the properties of Carbon web made from Acrylic waste, Strutex conference, December 2016. (Conference Paper)
5. V. Baheti, P. Behera, J. Militký, D. Karthik, Fly Ash Based Geopolymer Concrete Materials, Recent Developments in Fibrous Material Science, Pages 403-412. ISBN: 978-80-87269-45-9.
6. V. Baheti, P. Behera, D. Karthik, J. Militký, Properties of basalt fibres suitable in concrete composites, Advances in fibrous material science, Pages 95-118. ISBN: 978-80-87269-48-0.